



**© Copyright by Chinmay Shah**

**All Rights Reserved 2017**

**Virtual Synchronous Machine based Fuzzy V-F Control for VSC of Battery Storage  
System for Seamless Performance of Microgrid**

**A Thesis**

**Presented to**

**The Faculty of the Department of Electrical and Computer Engineering**

**University of Houston**

**In Partial Fulfillment**

**of the Requirements for the Degree**

**Masters of Science**

**In Electrical Engineering**

**By**

**Chinmay Shah**

**May 2017**

**Virtual Synchronous Machine based Fuzzy V-F Control for VSC of Battery Storage  
System for Seamless Performance of Microgrid**

---

**Chinmay Shah**

**Approved:**

---

Chair of the Committee  
Dr. Mehdi Abolhassani, Assistant Professor,  
Electrical and Computer Engineering,  
Electrical Engineering Technology

---

Dr. Heidar Malki, Professor,  
Electrical and Computer Engineering,  
Associate Dean, Engineering Technology

Committee Members:

---

Dr. Aaron Becker, Assistant Professor,  
Electrical and Computer Engineering

---

Dr. Xin Fu, Assistant Professor,  
Electrical and Computer Engineering

---

Dr. Suresh K. Khator, Associate Dean,  
Cullen College of Engineering

---

Dr. Badri Roysam, Professor and Chair,  
Electrical and Computer Engineering

## ACKNOWLEDGEMENT

First of all, I would like to express my sincere gratitude to my advisors, Dr. Mehdi Abolhassani and Dr. Heidar Malki, for the continuous support of Master's study and research, for their patience, motivation, enthusiasm, and immense knowledge. Their guidance helped me a lot to finish my research and writing of this thesis. I could not have imagined better advisors and mentors for my Master's study.

Besides my advisors, I would like to thank the rest of my thesis committee members Dr. Aaron Becker and Dr. Xin Fu for their encouragement, insightful comments, and positive feedback.

I would also like to show my appreciation to the department of Electrical and Computer Engineering for giving me the opportunity to be a part of well-organized program and provide me with resources to complete my research. My sincere thanks to Mr. Victor Gallardo, who supported me as Teaching Assistant throughout my tenure at University of Houston.

I thank my fellow lab mates at University of Houston: Prateek Gaure and Mehmet Akdogan for the stimulating discussions, for the sleepless nights we were working together before the deadlines, and for all the fun we had in the last two years.

Last but not the least, I would like to use this opportunity to thank my parents Dr. Bharat Shah and Chetna Shah for the priceless foundation they laid many years ago. None of these accomplishments would have been possible without their sacrifices. They are the best parents anyone could have wished for and I dedicate this thesis to them.

**Virtual Synchronous Machine based Fuzzy V-F Control for VSC of Battery Storage  
System for Seamless Performance of Microgrid**

**An Abstract**

**of a**

**Thesis**

**Presented to**

**The Faculty of the Department of Electrical and Computer Engineering**

**University of Houston**

**In Partial Fulfillment**

**Of the Requirements for the Degree**

**Masters of Science**

**In Electrical Engineering**

**By**

**Chinmay Shah**

**May 2017**

## **ABSTRACT**

This thesis presents seamless transition between the grid-connected and islanded mode of microgrid. The prominence of the seamless transition is to maintain the load voltage and frequency as well as constant power delivery during both the modes of operation of microgrid. In this thesis, voltage source converter (VSC) of PV generating unit operates in P-Q control mode in both grid-tied and islanded operation of microgrid due to its intermittent characteristics. The VSC of battery energy storage system (BESS) operates in P-Q control mode during grid-tied operation and in V-F control mode during islanded operation of microgrid. A fuzzy logic controller has been designed for V-F control during the islanded mode of operation of microgrid. The fuzzy logic controller can efficiently deal with non-linearity of power system as it does not depend on the mathematical model of the system. Also, the proposed fuzzy logic controller limits the switching transients as well as voltage swell and sags during the fault. The performance of fuzzy logic control is validated for seamless transition of microgrid from both the modes of operation through simulation in MATLAB/Simulink environment.

# TABLE OF CONTENTS

ACKNOWLEDGEMENT	v
ABSTRACT	vii
TABLE OF CONTENTS	viii
LIST OF FIGURES	xi
LIST OF TABLES	xiii
ACRONYMS	xiv
CHAPTER 1 INTRODUCTION	1
CHAPTER 2 MICROGRID: SYSTEM COMPONENTS AND LITERATURE REVIEW	5
2.1 Photovoltaic system	6
2.1.1 Photovoltaic Cell	6
2.1.1.1 Working of PV cell	7
2.1.2 Photovoltaic Module	8
2.1.3 Photovoltaic Array	8
2.2 Maximum Power Point Tracking	10
2.2.1 Algorithm for Maximum Power Point Tracking	11
2.2.2 MPPT Control	11
2.2.2.1 Perturb and Observe Technique	11
2.3 Battery Energy Storage System	14
2.3.1 Application of Battery Energy Storage System	15
2.4 Power Converters	15
2.4.1 DC-DC Converters	16



3.4 Microgrid Central Controller	65
3.4.1 Simulation Results	66
3.4.1.1 Case 3: Microgrid Load Management when Demand $[P_{load}] \leq$ Generation $[P_{GenTotal}$ $(P_{PV} + P_{Bat})]$	66
3.4.1.2 Case 4: Microgrid Load Management when Photovoltaic Generation $[P_{PV}] \sim 0$ kW & Battery Energy Storage System Power $[P_{Bat}] >$ Demand $[P_{Load}]$	69
3.4.1.3 Case 5: Microgrid Load Management when Photovoltaic Generation $[P_{PV}] \sim 0$ kW && Battery SOC $< 40\%$	71
CHAPTER 4 CONCLUSION	74
REFERENCES	75

## **LIST OF FIGURES**

Figure 2.1 Microgrid Generalized Model

Figure 2.2 Photovoltaic Cell

Figure 2.3 Photovoltaic System

Figure 2.4 Flowchart of Perturb and Observe Algorithm

Figure 2.5 Model of a Battery

Figure 2.6 DC-DC Boost Converter Model

Figure 2.7 Circuit Diagram of Boost Converter

Figure 2.8 Two Level Voltage Source Converter Topology

Figure 2.9 Voltage Source Converter Simulink Average Model

Figure 2.10 Schematic of Three Phase Two Pole Synchronous Generator

Figure 2.11 Block Diagram of Virtual Synchronous Machine Swing Equation

Figure 2.12 Simulink Model of Virtual Synchronous Machine Swing Equation

Figure 2.13 Architecture of Fuzzy Control

Figure 2.14 Generic Fuzzy Control Plant model

Figure 3.1 HOMER Load Profile Evaluation

Figure 3.2 Simulink Equivalent Model of PV Array

Figure 3.3 P-V Characteristics of PV Array

Figure 3.4 I-V Characteristics of PV Array

Figure 3.5 HOMER Simulation Tool Result for Battery Sizing and Calculation

Figure 3.6 Simulink Model of Microgrid Test System

Figure 3.7 Inner Control Loop for P-Q Control (PV Array)

Figure 3.8 Simulink Model of Inner Control Loop for P-Q Control

Figure 3.9 Outer Control Loop for P-Q Control

Figure 3.10 Simulink Block Diagram of P-Q Control for PV Generation Unit

Figure 3.11 Input Membership Function for Fuzzy Control

Figure 3.12 Fuzzy V-F Control Implementation Block Diagram

Figure 3.13 Block Diagram of Synchronization Control

Figure 3.14 Simulink Model of VSM based Fuzzy V-F Control

Figure 3.15 Case 1 Simulation Results

Figure 3.16 Case 2 Simulation Results

Figure 3.17 Simulink Model of Microgrid Central Controller

Figure 3.18 Irradiance and Temperature for 24 Hours Starting with 9<sup>th</sup> Hour of Day

Figure 3.19 Case 3 Simulation Results

Figure 3.20 Case 4 Simulation Results

Figure 3.21 Case 5 Simulation Results

## **LIST OF TABLES**

Table 2.1 Rule Base for Generic Fuzzy Controller

Table 3.1 Yearly Load Data (in kW)

Table 3.2 Power Dispatch in Month of August

Table 3.3 Power Dispatch in Month of December

Table 3.4 Fuzzy V-F Control Rule Base

Table 3.5 Microgrid Test Model Parameters

## ACRONYMS

V-F	Voltage and frequency
P-Q	Active and reactive power
PV	Photovoltaics
DG	Distributed generator
MPPT	Maximum power point tracking
P&O	Perturb and observe technique
DER	Distributed energy resource
VSC	Voltage source converter
VSM	Virtual synchronous machine
MF	Membership function
SOC	State of Charge
$P_{PV}$	Power from photovoltaic System
$P_{Bat}$	Power from Battery Energy Storage System
$P_{load}$	Load Power (Demand)
dq0	Direct-quadrature axis

## CHAPTER 1 INTRODUCTION

The emission of greenhouse gases due to the use of conventional energy resources for generation of power has led to climate change and this is critical issue faced by almost all the countries. Nowadays, renewable energy resource generators (PV array, wind turbine, hydro units, fuel cells etc.) are being installed at distribution level on a large scale. Due to this, higher requirement in voltage level, modular structure and flexibility as well as the reliability of the grid connected renewable energy generation resource inverter have been put forward. The features are as follows:

- 1) Peak power capacity: Renewable energy sources should be able to store the electrical energy during the Off-peak hours, while this stored energy can be utilized to feed the load during the peak hours. As a result, the peak power of the grid and the reliability of the power supply can be improved.
- 2) Fault ride through capacity: A large scale renewable energy system should have the ability to withstand short periods of voltage abnormality caused by short circuit fault.
- 3) Power quality control: More stable power performance could be achieved by introducing suitable inverter control strategy including voltage stability, phase and frequency regulation etc.
- 4) Redundant operation and error correction capacity: The renewable energy system should have the capacity to work efficiently during the failure of inverter system and smart enough to retrieve to its default operation.

In order to fulfill all the above-mentioned requirements, the concept of the microgrid has been introduced. As per U.S. Department of Energy, a microgrid is a group of

interconnected loads and distributed energy resources (DER) with clearly defined electrical boundaries that acts as a single controllable entity with respect to the grid [and can] connect and disconnect from the grid to enable it to operate in both grid-connected or island mode[1]. Microgrid enables high penetration of renewable energy distributed generating (DG) units to the utility grid without any notable changes in the utility grid. Microgrid also enhances local reliability by reducing feeder losses, feed local critical loads during fault/blackout, voltage sag correction etc. The integration between microgrid and utility grid must meet the interconnection standards (IEEE 1547) to ensure that the power flowing through the point of common coupling is smooth [2]. Microgrid can operate in two modes: 1) Grid connected mode and 2) Islanded/Autonomous mode. During severe fault condition in the main grid, the microgrid detach itself from the main grid and operates in islanded mode. It reconnects to the main grid as soon as the fault is clear in the utility grid. Seamless transition of microgrid between the two modes of operation is important to ensure minimal disruption to the critical loads. Seamless transition of microgrid means smooth and continuous interconnection of microgrid with the utility grid and within IEEE 1547 standard (voltage fluctuation within +10% and frequency variation between 59.3Hz and 60.5 Hz).

There are several issues that needs to be taken into consideration for seamless transition of microgrid from both the modes of operation. The following are some of the many issues that are considered in this thesis for seamless transition of a Microgrid:

- 1) Control Strategy: The renewable energy resource DG units and energy storage systems in Microgrid are interfaced to the main grid through power electronic converters. A proper control strategy needs to be proposed to control the output

voltage and frequency of the power electronic converter to synchronize microgrid with the utility grid. Voltage source converter (VSC) operates in P-Q control mode while the microgrid is grid connected or V-F control mode while microgrid is operating in islanded mode. The active power generated by renewable energy resource DG units has weather dependent restrictions, it is not suitable for VSC renewable energy resource DG units to operate in V-F control mode during islanded operation. Any system with constant active power like battery energy storage system (BESS) VSC should be asked to operate in V-F control mode to maintain voltage and frequency during islanded mode of operation of microgrid. In [3] – [4], droop controller is designed for seamless transition of microgrid between both the modes of operation. However intermittent characteristics of renewable energy resource DG units as discussed above have not been taken into consideration while designing a controller for VSC in these papers.

In [5] multivariable control system is applied for islanded mode of operation of microgrid, but the controller design is complex and depends on the state space model of the microgrid. A PI controller is used in [6] for seamless transition of microgrid, but PI controller suffer from sensitivity to parameter variation and system non-linearity.

All the limitations and issues existing in these control strategies have been taken into consideration while proposing a new control strategy for seamless transition of microgrid in this thesis. Decentralized fuzzy logic control strategy for BESS has been proposed in this work. Fuzzy logic controller (FLC) has improved performance over conventional control strategies and present an alternative

approach in controlling the systems that exhibit high degree of uncertainty. There are many advantages of FLC: a) It can effectively deal with nonlinear systems. b) It does not need the mathematical model of the system and c) FLC can result in better performance, when fine-tuned, than the conventional controllers.

- 2) Microgrid Synchronization: There is presence of nonlinear unbalanced loads as well as renewable energy resource DG's with intermittent characteristics in microgrid. All of them are interfaced to the grid through voltage source converters. In islanded operation of microgrid, all voltage source converter present in the microgrid do not need any external reference to stay synchronized. In fact, they can operate in parallel with other VSC by using frequency and voltage droops. But before microgrid is reconnected to the main grid, it needs to be synchronized with main utility grid's frequency, phase and amplitude.
- 3) Load Management: Load management is one of the technical challenge while planned or unplanned conversion of microgrid form grid-tied mode to islanded mode. Due to intermittent characteristics of renewable energy resource DGs present in microgrid, it might not be possible to feed all the loads sufficiently during the islanded operation of microgrid. Load shedding control strategy needs to be proposed in order to detect non-critical loads in the islanded microgrid and isolate them.

As a part of this thesis work, the proposed virtual synchronous machine based fuzzy V-F control with cascade synchronization controller will provide solution to all the issues discussed above and is simulated using MATLAB/Simulink environment.

## CHAPTER 2 MICROGRID: SYSTEM COMPONENTS AND LITERATURE REVIEW

The U.S. Department of Energy defines microgrid as a group of interconnected loads and distributed energy resources (DER) with clearly defined electrical boundaries that acts as a single controllable entity with respect to the grid and can connect or disconnect from the grid to enable it to operate in both grid-connected or island mode [1]. A generalized model of microgrid is shown in figure 2.1 which consists of one DER e.g. PV generation unit and one battery energy storage system. The battery energy storage system is quintessential to maintain power flow in DER based microgrid.

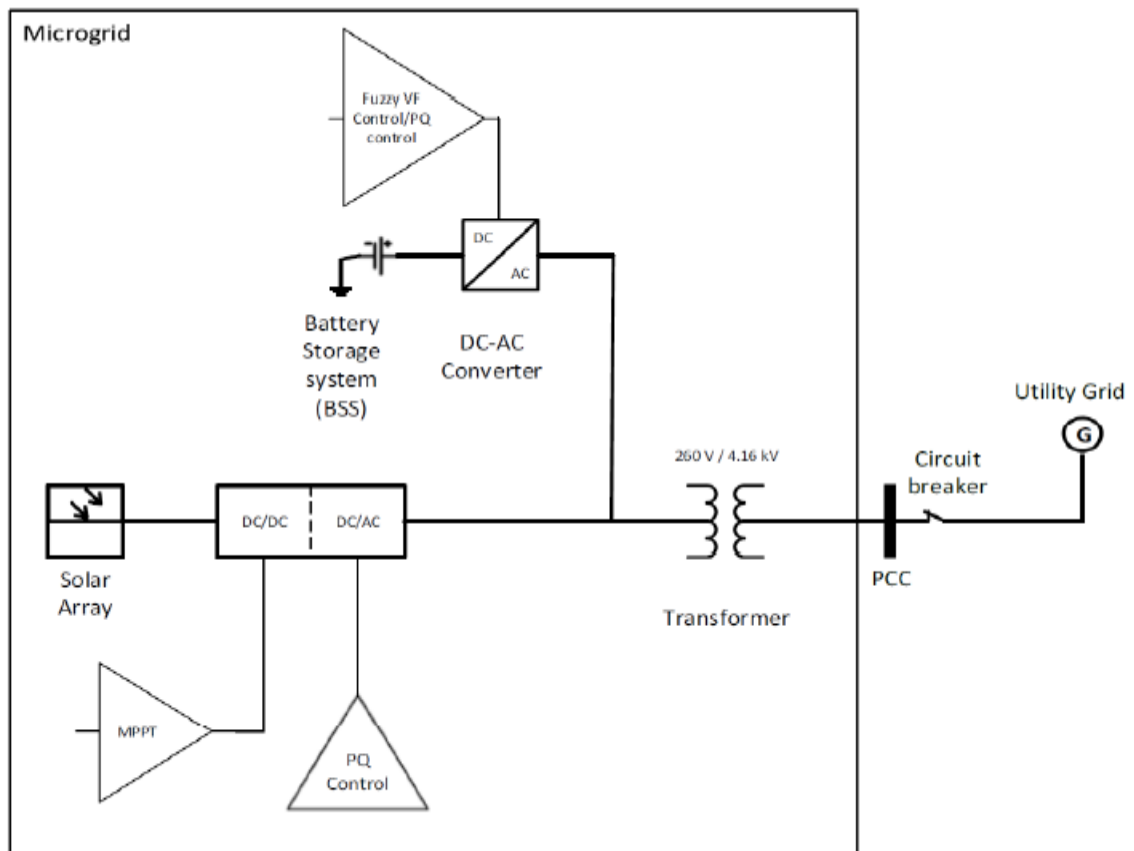


Figure 2.1 Microgrid Generalized Model

The DER and energy storage system in microgrid is connected to the grid at PCC through power electronic converters. It can operate in both grid connected and islanded mode. The control of power electronic interfaced DER and energy storage system depends on the mode of operation of microgrid. This chapter gives a brief explanation about all the components in microgrid including DER, battery energy storage system, power electronic converters and various control topologies. The concept of virtual synchronous machine is also described in this chapter, which is a part of proposed control topology in this thesis.

## **2.1 Photovoltaic System**

The photoelectric effect was first noted by French physicist Edmund Becquerel in 1839. He proposed that certain materials have property of producing small amounts of electric current when exposed to sunlight. The principle of photovoltaic technology is based on the theory proposed by Albert Einstein on composition of light and photoelectric effect. In 1954 the first photovoltaic module was built by Bell Laboratories [7].

The main aim of photovoltaic technology is to convert solar energy into electrical energy or electricity. It consists of number of solar panels which are composed of number of series and parallel photovoltaic modules. The photovoltaic modules are assembled solar cells.

### **2.1.1 Photovoltaic Cell**

The conventional photovoltaic or solar cells are made from crystalline silicon such as polysilicon or monocrystalline silicon. The modern day solar/photovoltaic cells are manufactured from amorphous silicon, CdTe (cadmium telluride) and CIGS (copper, indium, gallium, selenide). When light energy hits the solar cell, electrons are knocked loose from the atoms in the semiconductor material. When electrical conductors are

connected to the positive and negative sides an electrical circuit is formed and electrons are captured in the form of an electric current that is, electricity. A PV cell can either be circular or square in construction [7]. The schematic of PV cell is shown in figure 2.2.

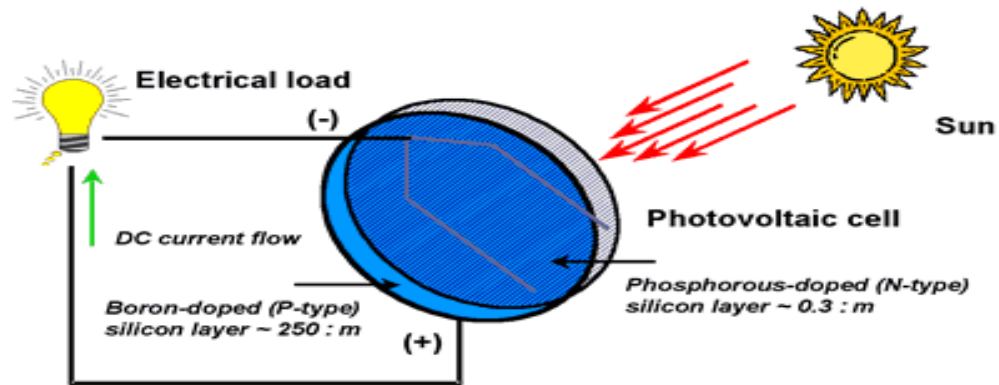


Figure 2.2 Photovoltaic Cell [Jignesh patel – Quora]

### 2.1.1.1 Working of PV Cell

The PV cell functions on the principle of photoelectric effect. When sunlight is incident on solar cell, it absorbs the photons of certain wavelength and energize the electrons to jump from valence band to conduction band. Hence when low temperature, low irradiance is incident on solar cell, it will not generate any electricity because electrons will not be energized enough to jump from valence band to conduction band.

The electron from valence band jumps to the conduction band when absorbed energy is greater than the band gap energy of the semiconductor. This creates hole-electrons pairs in the illuminated region of the semiconductor. The electrons created in the conduction band are now free to move. These free electrons are enforced to move in a particular direction by the action of electric field present in the PV cells and forms electric current. This electric current can be drawn for external use by connecting a metal plate on

the top and bottom of a PV cell. The product of current and the potential difference between two plates produces required power [7].

### 2.1.2 Photovoltaic Module

The low voltage generation in a PV cell (around 0.5V) limits its usage. Hence several PV cells are connected in series and in parallel to form a PV module for its commercial usage. Usually there are of 36 or 72 cells in general PV modules. The module is made from tempered glass on the front side to make it transparent, encapsulated silicon wafer and back side.

### 2.1.3 Photovoltaic Array

A photovoltaic array (PV system) is an interconnection of modules which in turn is made up of many PV cells in series or parallel [7].

The figure 2.3 represents how PV array is formed.

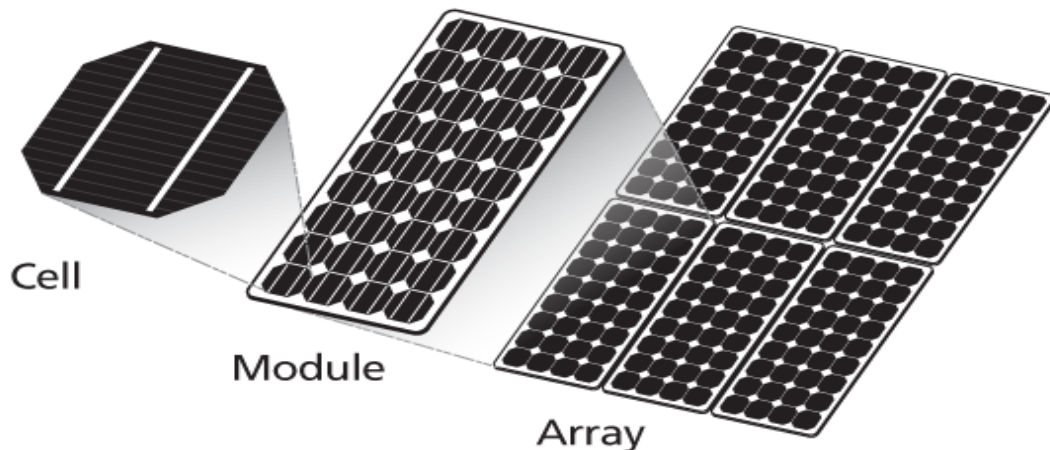


Figure 2.3 Photovoltaic System [Samlex solar]

The circuit of a PV array consists of a diode and a parallel resistor which expresses a leakage current, and a series resistor which describes an internal resistance to the current

flow. The mathematical equations that describe the V-I characteristics of the ideal PV array are

$$I = I_{pvcell} - I_d \text{ and } I_d = I_{ocell} \left[ \exp\left(\frac{qV}{akT}\right) - 1 \right], \quad (2.1)$$

where  $I_{pvcell}$  (A) is the current generated by the incident light,  $I_d$  is the Shockley diode equation,  $I_{ocell}$  (A) is the reverse saturation or leakage current of the diode,  $q$  is the electron charge ( $1.60217646 \times 10^{-19}$  C),  $K$  is the Boltzmann constant ( $1.3806503 \times 10^{-23}$  J/K),  $T$  (K) is the working temperature of p-n junction and  $a$  is the diode ideality factor.

$$I = I_{pv} - I_0 \left[ \exp\left[\frac{V+R_s I}{aV_t}\right] - 1 \right], \quad (2.2)$$

where  $I_{pv}$  (A) and  $I_0$  (A) are the photovoltaic and saturation currents of the array and  $V_t = (N_s K T)/q$  is the thermal voltage of the array with  $N_s$  cells in series,  $R_s$  and  $R_p$  are the equivalent series and parallel resistance of the array.

$$I_{pv} = (I_{pvn} + K_I \Delta T) \times \left(\frac{G}{G_n}\right), \quad (2.3)$$

where  $I_{pvn}$  (A) is the light generated current at the nominal condition (usually 25°C and 1000W/m<sup>2</sup>),  $\Delta T = T - T_n$ ,  $G$  (w/m<sup>2</sup>) and  $G_n$  (W/m<sup>2</sup>) are the operating and nominal irradiation,  $K_I$  is current/temperature coefficient in A/K.

The diode saturation current  $I_0$  mainly depends on the temperature given by,

$$I_0 = (I_{scn} + K_I \Delta T) / \left[ \exp\left\{\frac{V_{ocn} + K_v \Delta T}{aV_t}\right\} - 1 \right], \quad (2.4)$$

where  $I_{scn}$  (A) a nominal short circuit is current,  $V_{ocn}$  (V) is the nominal open circuit voltage and  $K_v$  is the voltage/temperature coefficient in V/K.

If the photovoltaic array is composed of  $N_{ser}$  series and  $N_{par}$  parallel modules then,

$$I = I_{pv}N_{par} - I_0N_{par} \left[ \exp \left\{ \frac{V + R_s \left( \frac{N_{ser}}{N_{par}} \right) I}{aV_t N_{ser}} \right\} - 1 \right], \quad (2.5)$$

and array maximum power output is given by

$$P_{MPP} = V_{MPP} \times I_{MPP}. \quad (2.6)$$

## 2.2 Maximum Power Point Tracking

The output of photovoltaic system is dependent on several factors like temperature, irradiance, and load characteristics. Since all these factors are intermittent in nature, the output of PV system is different for different time interval and hence it reduces its overall efficiency to about 13 %. As the module efficiency is low, it is desirable to operate the module at peak power point so that maximum power can be delivered to the load under varying temperature and irradiation conditions. For this reason, the maximum power point tracker (MPPT) is required to track the output of PV system. It is an electronic system that tracks a suitable operating point of PV module and sends a control signal to DC-DC converter to transfer maximum power from solar PV module to the load.

### 2.2.1 Algorithms for Maximum Power Point Tracking

The different algorithms that can track the maximum power point of the solar PV module are:

- a. Perturb and observe
- b. Incremental conductance
- c. Parasitic capacitance
- d. Voltage based peak power tracking
- e. Current based peak power tracking

## 2.2.2 MPPT Control

The role of MPPT control in PV system is to automatically track the voltage  $V_{MPP}$  or the current  $I_{MPP}$  at which the PV array should operate to obtain the maximum power o/p  $P_{MPP}$  under a given operating temperature and irradiance. Most MPPT techniques respond to changes in both irradiance and temperature. In this thesis work perturb and observe technique is used for MPPT control.

### 2.2.2.1 Perturb and Observe Technique

In this algorithm, a slight perturbation is introduced in the system. The power of the module changes due to this perturbation. If the power increases due to the perturbation, then the perturbation is continued in that direction [7]. When power attains its peak point, it starts to decrease at next instant and hence the need to reverse the perturbation. During the steady state condition the algorithm oscillates around the peak point. The perturbation size is kept very small to keep the power variation small. It is examined that there is some power loss because of this perturbation and also it fails to track the power under fast varying atmospheric conditions. The Figure 2.4 represents flow chart of the algorithm.

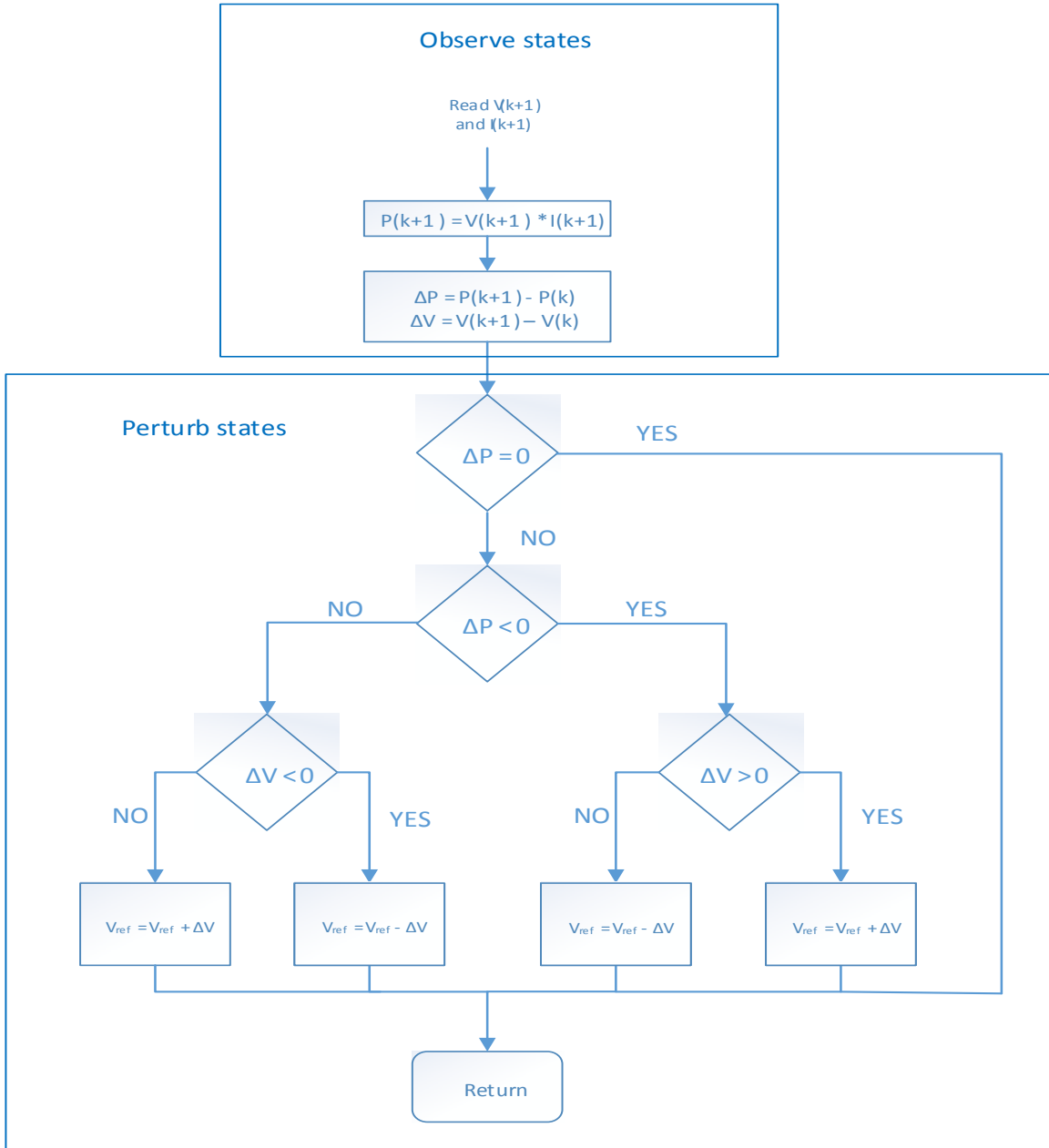


Figure 2.4 Flowchart of Perturb and Observe Algorithm

The output voltage and power of the array is measured and the algorithm perturbs the power based on increment of the array voltage. Based on the measured value of power in previous time step, it tries to increase or decrease the reference value of the voltage. The reference value of the voltage  $V_{ref}$  is set corresponding to the maximum power point of the module. From the measured value of voltage and current from PV module, power of

PV system is calculated. The value of voltage and power at  $k^{th}$  instant and at  $(k + 1)^{th}$  instant is measured and compared. If we observe the power voltage curve of the solar PV module we see that in the right-hand side curve where the voltage is almost constant. The slope of power voltage is negative ( $dP/dV < 0$ ) where as in the left hand side the slope is positive ( $dP/dV > 0$ ). Depending on the sign of  $dP[P(k + 1) - P(k)]$  and  $dV[V(k + 1) - V(k)]$  after subtraction, the algorithm decides whether to increase or to reduce the reference voltage [7].

The P&O method is claimed to have slow dynamic response and high steady state error. In fact, the dynamic response is low when a small increment value and a low sampling rate are employed. To decrease the steady state error low increments are essential because the P&O always makes the operating point oscillate near the MPP, but never at the MPP exactly [7]. When the increment is lower, the system will be closer to the array MPP. In case of greater increment, the algorithm will work faster, but the steady state error will be increased. The small increments tend to make the algorithm more stable and accurate when the operating conditions of the PV array change. In case of large increments the algorithm becomes confused since the response of the converter to large voltage or current variations will cause oscillations, overshoot and the settling time of the converter itself will confuse the algorithm [7].

## 2.3 Battery Energy Storage System

The output of battery depends not only on the current but also on the battery state of charge (SOC), which is a nonlinear function of the current and time. Hence the model of battery is always designed as nonlinear. The figure 2.5 represents a basic model of battery.

The original Shepherd model has a non-linear term equal to  $k \frac{Q}{Q - \int i dt} i$ . This term represents a non-linear voltage that changes with the amplitude of the current and the actual charge of the battery. When there is complete discharge of battery and no flow of current, the voltage of the battery will be nearly zero. As soon as a current circulates again, the voltage falls abruptly. This model yields accurate results and also represents the behavior of the battery.

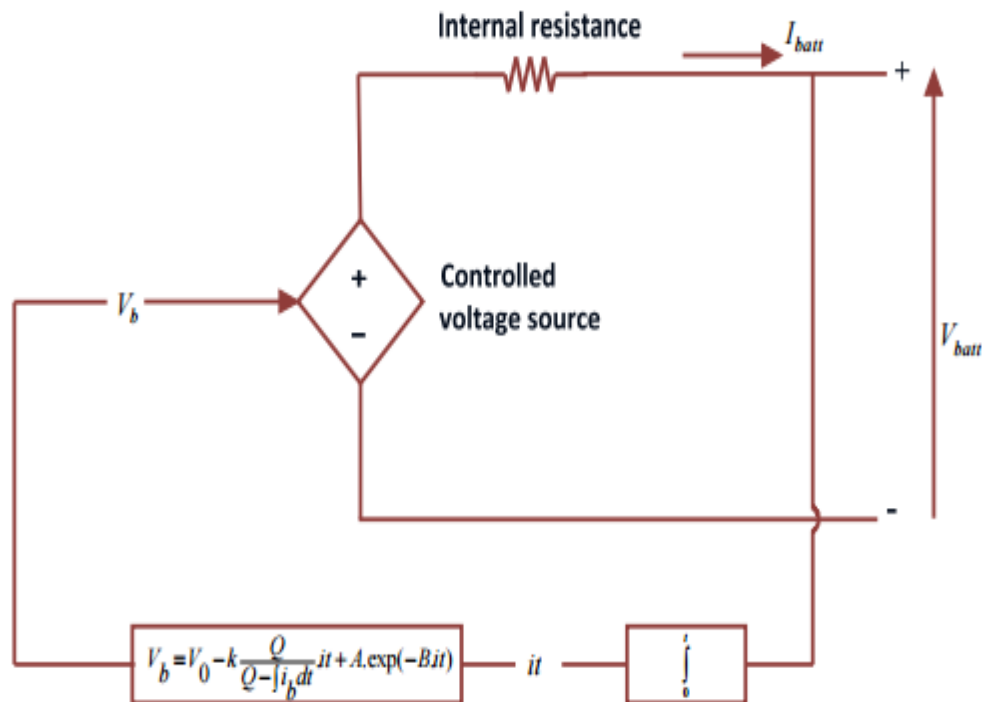


Figure 2.5 Model of Battery.

### **2.3.1 Applications of Battery Energy Storage System**

This section presents the application explicitly targeting increased integration of distributed renewables.

- 1) Renewable energy time shift/spinning reserve
- 2) Capacity firming/ramp support/forecast hedging
- 3) Voltage support/voltage stability
- 4) Increasing hosting capacity
- 5) Arbitrage/electric energy time shift
- 6) Demand charge reduction
- 7) Customer power reliability and quality
- 8) Load shedding and area regulation
- 9) Voltage support
- 10) Transmission support and frequency regulation
- 11) Peak shaving to minimize grid losses
- 12) Transmission congestion relief and upgrade deferral

### **2.4 Power Converters**

The distributed energy resources (DER) are the backbone of modern power grid. DERs are nothing but renewable energy generation sources and energy storage devices. Just as synchronous machines plays an important role in conventional power system, power electronic converters are important for flexible, efficient and seamless interconnection of DERs in modern distributed grid.

The main aim of using power electronic converters is to process electric power from DER by electronic devices which have a controllable behavior. Various basic functions

may be performed by power electronic converters. Based on their function, they can be classified in to four basic types [10]: 1) AC to DC converters or rectifiers, 2) DC to DC converters. 3) AC to AC converters and 4) DC to AC converters or Inverters. From four types of converters mentioned above, only DC-DC converters and DC-AC converter or inverters are discussed in this research work. DC-DC converters are fed with DC voltage and the output would be DC voltage with value either higher or lower than input DC voltage and different polarity. DC-AC converters or inverters are devices that transform DC voltage into 3 phase AC voltage with variable magnitude and frequency. The power flow through both the converters can be bidirectional i.e. interchanging the role between the input and output ports.

### **2.4.1 DC-DC Converters**

DC-DC converters are used when we want to change the amplitude of voltage from one level to another. The need for such converters have increased due to the fact that transformers are unable to step up or step down DC voltage. There are three different topologies for DC-DC converters: 1) Buck Converter, 2) Boost Converter and 3) Buck-Boost Converter. We will discuss about the boost converter and bidirectional buck-boost converter which are used to integrate PV array and battery energy storage system on the DC bus respectively in this research work.

#### **2.4.1.1 Boost Converter (Average Model)**

A boost converter steps up the DC voltage as its name suggests. This converter consists of a diode D, a transistor or MOSFET as switch S and storage element capacitor C.

The figure 2.6 shows the model of DC-DC boost converter [11] and [12].

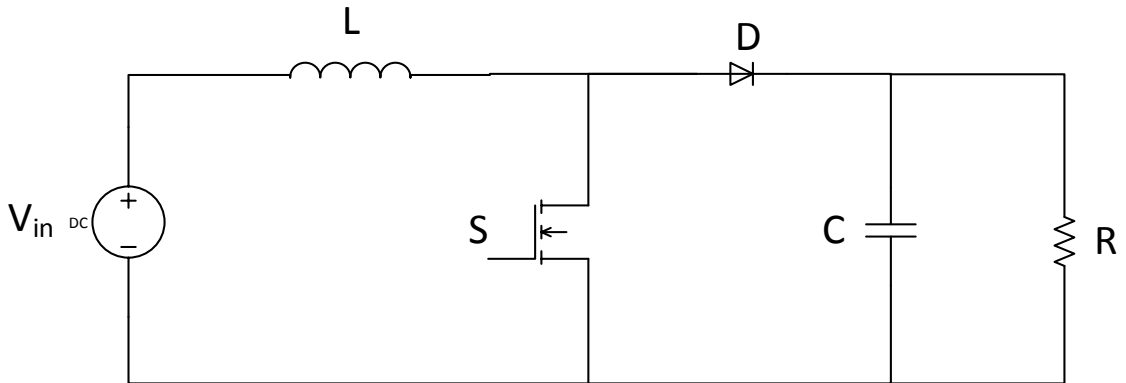


Figure 2.6 DC-DC Boost Converter Model

There are two state of operation:

- 1) When the transistor or MOSFET S is ON, diode D will be inversely polarized and there will be no connection between source input and the load. The circuit diagram for this topology is shown in figure 2.7(a).
- 2) When the transistor or MOSFET is OFF, diode D will be conducting and power will flow from input source to the load. The circuit diagram for this state is shown in figure 2.7(b).

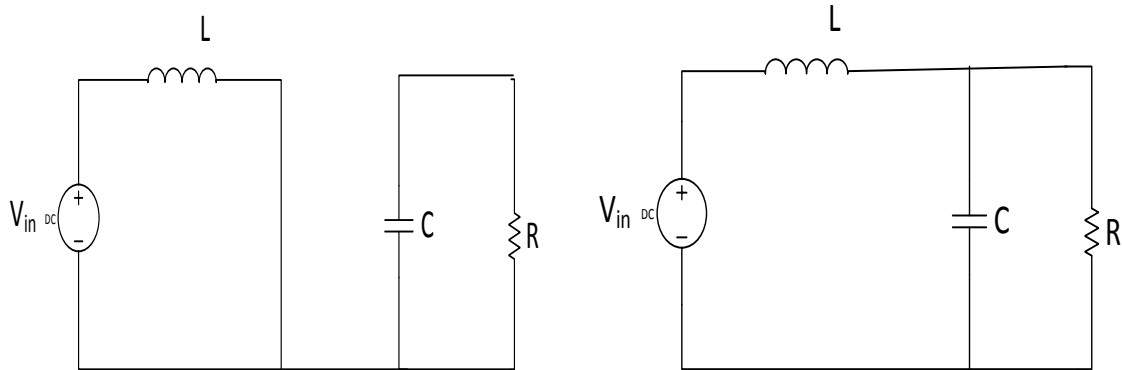


Figure 2.7 (a) Switch S is "ON"

(b) Switch S is "OFF"

Now let  $D$  be the duty cycle and  $T$  be the time period of one cycle. The switch  $S$  will be in ON state for  $T_{on} = D \cdot T$  and switch  $S$  will be OFF for  $T_{off} = (1-D) \cdot T$ . When switch is ON the voltage between the terminals of the inductor is,

$$V_L = V_{IN} - I_L \times ((R_{ON} \times D) + R), \quad (2.7)$$

where  $R$  is the load resistance,  $I_L$  is inductor current,  $V_{IN}$  is input voltage and  $V_L$  is voltage across inductor [13].

The value of the inductor is calculated using the equation,

$$L = \frac{V_{IN} \times (V_{OUT} - V_{IN})}{\Delta I_L \times f_s \times V_{OUT}}, \quad (2.8)$$

where  $\Delta I_L$  is inductor ripple current,  $V_{OUT}$  is output voltage of boost converter,  $f_s$  is switching frequency of the converter. Now good estimation of inductor ripple current is 20% to 40% of the output current,

$$\Delta I_L = (0.2 \text{ to } 0.4) \times I_{OUT} \times \frac{V_{OUT}}{V_{IN}}, \quad (2.9)$$

The value for the output capacitor is calculated using the equation,

$$C = \frac{I_{OUT(max)} \times D}{f_s \times \Delta V_{OUT}}, \quad (2.10)$$

where  $I_{OUT(max)}$  is maximum output current and  $\Delta V_{OUT}$  is the desired output voltage ripple.

The ESR (equivalent series resistance) of the output capacitor adds some more ripple. The output voltage ripple is given by,

$$\Delta V_{OUT(ESR)} = ESR \times \left( \frac{I_{OUT(max)}}{1-D} + \frac{\Delta I_L}{2} \right). \quad (2.11)$$

When switch  $S$  is OFF state, the voltage across inductor will be

$$V_L = V_{IN} - (V_{OUT} + V_D), \quad (2.12)$$

where  $V_D$  is the voltage across diode.

Now after all the calculations have been performed for the components required to design boost converter, the converter circuits shown in figure 4.2 can be represented in form of equation using Kirchhoff's voltage and current law. For switch S is ON (=1), following set of equations are obtained,

$$L \frac{dI_L}{dt} = V_{IN} \text{ and} \quad (2.13)$$

$$C \frac{dV_{OUT}}{dt} = -\frac{V_{OUT}}{R}. \quad (2.14)$$

For switch S is OFF (=0), following set of equations are obtained

$$L \frac{dI_L}{dt} = -V_{OUT} + V_{IN} \text{ and} \quad (2.15)$$

$$C \frac{dV_{OUT}}{dt} = I_L - \frac{V_{OUT}}{R}. \quad (2.16)$$

Both the states can be described together by combining equations from 2.13 to 2.16. Thus, the combined dynamics of boost converter is represented by,

$$L \frac{dI_L}{dt} = -(1 - S) \times V_{OUT} + V_{IN} \text{ and} \quad (2.17)$$

$$C \frac{dV_{OUT}}{dt} = (1 - S) \times I_L - \frac{V_{OUT}}{R}. \quad (2.18)$$

The average model for boost converter can be designed based on above state space equations. In this research work the duty cycle D to control the switching action is fed by MPPT controller, which is discussed in previous section. MPPT controller tries to maintain the output voltage and power of PV generator on DC bus through DC-DC boost converter.

## 2.4.2 DC-AC Converter/ Inverter

The main function of DC-AC converter or voltage source converter or inverter is to transform DC voltage to a symmetric output AC voltage of desired voltage and frequency. The output voltage waveforms of ideal inverter should be sinusoidal. However, the output waveforms of practical inverters contains harmonics and hence are non-sinusoidal. The harmonic content of the output voltage can be minimized by LCL filter or using higher switching frequency. Inverters play a major role in modern power grid to integrate energy storage system and renewable energy sources to the AC grid. Two level voltage source converters are used in this research work to integrate PV array generation system and battery energy storage system. The topology for two level converter is represented in figure 2.8 [14].

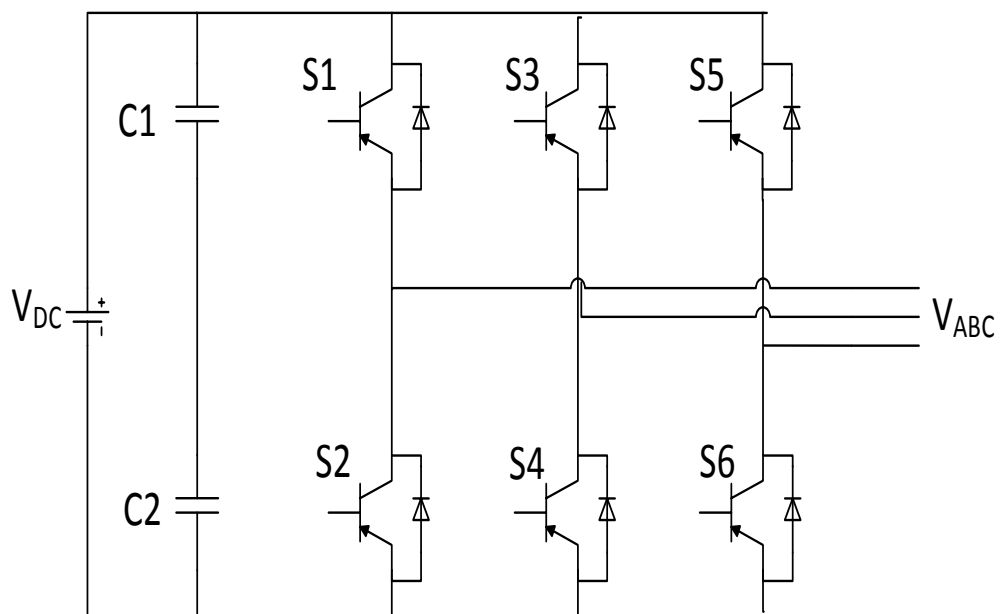


Figure 2.8 Two Level Voltage Source Converter Topology

As shown in figure 2.8, two level voltage source converter consist of 6 IGBT switches (S1-S6). The parameters taken into account while designing and specifying IGBT switches are

high blocking voltage and turn off current, low conduction and switching losses, short turn-on and turn-off times, suitable for series connection, high dv/dt & di/dt withstand capability, good thermal characteristics and low failure terms.

Now for the two level converter model shown above, depending on whether the upper or lower switches are conducting, each phase terminal can be connected to either positive or negative terminal of the input DC voltage. The switches of any leg of the inverter (S1 and S2, S3 and S4, S5 and S6) cannot be switched on simultaneously; this would result in short circuit across the DC-link voltage supply. The switching frequency of the switches in two level power converter is of the order of several kHz for high power applications.

#### **2.4.2.1 Voltage Source Converter (Average Model)**

For power electronic converters, the phase current consists of the fundamental sine component with the superimposed high-frequency switching ripples. The average model makes an assumption that the ripple due to switching can be ignored. Hence, instead of looking at the instantaneous values of currents and voltages that contain high frequency ripple, a dynamic average-value that is defined over the switching interval  $T_s$  could be used:

$$\bar{f}(t) = \frac{1}{T_s} \int_{t-T_s}^t f(s) ds, \quad (2.19)$$

where  $\bar{f}(t)$  represent either voltage or current,  $T_s$  is switching period [14].

However, just averaging of the AC variables using the equation 2.19 over the switching period will not yield the desired result. In this case, the AC side variables must be expressed

in an appropriate synchronously rotating dq0 reference frame in order to transform them to constant dc parameters. The voltages on the AC and DC side can be expressed as follows,

$$\|V_{dq}\| = \sqrt{V_d^2 + V_q^2} = \alpha V_{dc}, \quad (2.20)$$

where  $\alpha$  is an algebraic function.

Similarly the current on AC and DC side can be expressed as:

$$I_{dc} = \beta \|I_{dq}\| = \beta \sqrt{I_d^2 + I_q^2}, \quad (2.21)$$

where  $\beta$  is another algebraic function. Both  $\alpha$  and  $\beta$  depend on the type of inverter and the operating conditions.

Now looking at the AC side, the three phase power can be expressed as

$$P_{ac} = \frac{3}{2} \|V_{dq}\| \cdot \|I_{dq}\| \cos(\phi), \quad (2.22)$$

where  $\phi$  is the power factor angle. By the principle of power conservation principle, the power on the DC and AC side are equal. Thus DC bus current can be expressed as,

$$I_{dc} = \frac{P_{ac}}{V_{dc}} = \frac{3}{2} \alpha \cos(\phi) \cdot \|I_{dq}\|. \quad (2.23)$$

It is clear from equations 2.21 and 2.23 that  $\beta = \frac{3}{2} \alpha \cos(\phi)$ .

The value of algebraic function  $\beta$  depends on the load value since it is dependent on cos factor angle  $\phi$ . The angle is expressed in terms of dq0 components as follows:

$$\phi = \tan^{-1}\left(\frac{V_d}{V_q}\right) - \tan^{-1}\left(\frac{I_d}{I_q}\right). \quad (2.24)$$

The average model of two level voltage source converter calculates the AC voltage from the reference signal generated by the control system and DC voltage is available from DC

side measurements. The AC side currents become the input of the average model and are derived from the network model on the AC side. The DC current is calculated as a function of the algebraic function  $\alpha$  and the AC currents in the dq0 frame. The figure 2.9 shows the simulink model of voltage source converter average model.

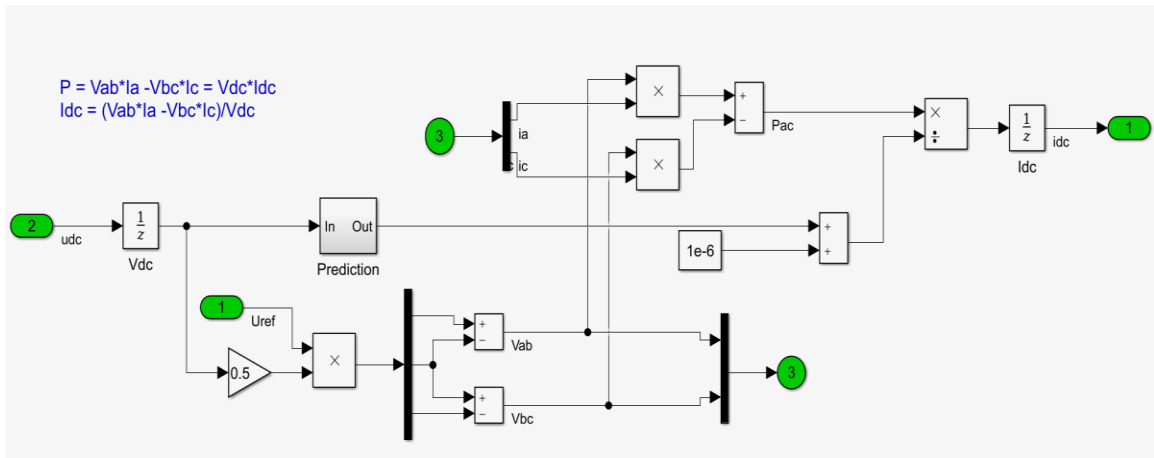


Figure 2.9 Voltage Source Converter Simulink Average Model

The average model is useful for design of controllers and analysis of dynamic interactions of converter circuits. Also PWM generator is not required to control average model and it provides the fastest simulation. Control techniques will be discussed in next chapter of this research work.

## 2.5 Virtual Synchronous Machine

The power grid mainly relies on conventional power generation system which consists of large synchronous generators. These synchronous generators generate power at certain frequency and it tries to maintain the grid frequency by varying its speed under abnormal or fault conditions for stable operation. Now certain loads or renewable energy generation sources are connected to the grid through voltage source inverters. These inverters are designed to follow the grid's frequency and phase since it does not have its

own inertia to maintain the frequency and synchronize with other generators and load connected to the grid.

Nowadays, due to the improvisation in renewable energy technology, more and more renewable energy generation systems like solar and wind are penetrated in to the power grid. The increasing percentage of power electronic based renewable energy generation system in the grid can lead to loss of inertia in the system, which in turn can cause frequency instability in the grid as well as deteriorate the power quality. Hence it is very important to develop control strategies for power electronic converters, which will allow renewable energy generation sources to participate in grid frequency and output power control like synchronous generators. The control technique based on Virtual Synchronous Machine will allow voltage source converters to emulate the dynamic performance of conventional synchronous generator. In this research work, virtual synchronous machine based fuzzy control technique is developed for stable operation of microgrid in grid connected as well as islanded mode and its seamless switching between both the modes of operation. This control technique will be discussed in detail in next chapter. This chapter is divided two sections, first sections explains the function of conventional synchronous generator, while second section explains the design and performance of virtual synchronous generator.

### **2.5.1 Synchronous Generator**

Synchronous generators are synchronous machines used to convert mechanical power to AC electric power. Most of world's power system are three-phase system and hence synchronous generators are three phase machines [14] and [15]. For the production of a set of three voltages phase-displaced by  $120^\circ$  in time, a minimum of three coils phase-

displaced  $120^\circ$  in space must be used. In addition to these windings, synchronous generator rotor contains damper windings which come into effect in machine's transient state of operation. The figure 2.10 displays a simplified schematic view of a three-phase, two-pole machine with one coil per phase.

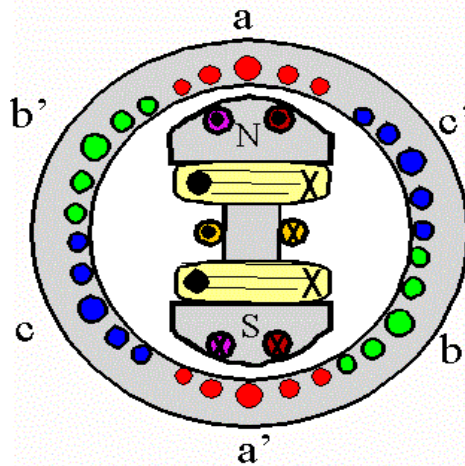


Figure 2.10 Schematic of Three-Phase Two-Pole Synchronous Generator

In a synchronous generator, rotor is rotated by the prime mover, which produces the rotating magnetic field within the machine. As the rotor rotates, the flux linkages of the armature winding change with the time. Under the assumption of a sinusoidal flux distribution and constant rotor speed, the resulting coil voltage will be sinusoidal in time. The coil voltage passes through a complete cycle for each revolution of the two-pole machine of figure 2.10 [15, 16]. Its frequency in cycles per second (Hz) is the same as the speed of the rotor in revolutions per second: the electric frequency of the generated voltage is synchronized with the mechanical speed, and this is the reason for the designation "synchronous" machine [15, 16]. Thus a two-pole synchronous machine must revolve at 3600 revolutions per minute to produce a 60-Hz voltage.

In this thesis work, three important characteristics of synchronous generator, which are very pivotal in the stable and reliable operation of power system are taken into consideration. The three important features are as follows:

- 1) Inertia in synchronous generator due to the rotating masses
- 2) Damping effect due to the damper windings in the rotor
- 3) Speed-droop characteristics of a synchronous generator for load sharing.

The equation of motion of the rotor of synchronous generator, which is driven by prime mover is given by

$$J \frac{d\omega_m}{dt} + D_d \omega_m = \tau_t - \tau_e, \quad (2.25)$$

where  $J$  is the total moment of inertia of the turbine and the generator rotor,  $\omega_m$  is the rotor shaft velocity,  $\tau_t$  is the torque produced by the turbine,  $\tau_e$  is the counteracting electromagnetic torque and  $D_d$  is the damping torque coefficient and accounts for the mechanical rotational loss due to wind age and friction [15].

Although the turbine torque  $\tau_t$  changes relatively slowly, due to the long thermal time constants associated with the boiler and turbine, the electromagnetic torque  $\tau_e$  may change its value most instantaneously. In the steady state the rotor angular speed is synchronous speed  $\omega_{sm}$  while the turbine torque  $\tau_t$  is equal to the sum of the electromagnetic torque  $\tau_e$  and the damping torque  $D_d \omega_{sm}$

$$\tau_t = \tau_e + D_d \omega_{sm} \text{ or} \quad (2.26)$$

$$\tau_m = \tau_t - D_d \omega_{sm} = \tau_e, \quad (2.27)$$

where  $\tau_m$  is the net mechanical shaft torque, which is the turbine torque less the rotational losses at  $\omega_m = \omega_{sm}$ . It is this torque that is converted into electromagnetic torque [15, 16].

If due to some disturbance,  $\tau_m > \tau_e$  then the rotor accelerates; if  $\tau_m < \tau_e$  then it decelerates. The rotor velocity can now be expressed as

$$\omega_m = \omega_{sm} + \Delta\omega_m. \quad (2.28)$$

The swing equation for the rotor will be modified as

$$J \frac{d\omega_m}{dt} + D_d \Delta\omega_m = \tau_m - \tau_e. \quad (2.29)$$

Multiplying the equation by rotor synchronous speed  $\omega_{sm}$  gives

$$J\omega_{sm} \frac{d\omega_m}{dt} + D_d \omega_{sm} \Delta\omega_m = \omega_{sm} \tau_m - \omega_{sm} \tau_e. \quad (2.30)$$

As power is the product of angular velocity and torque, the terms on the right hand side of the equation 2.30 can be expressed in terms of power to give

$$J\omega_{sm} \frac{d\omega_m}{dt} + D_d \omega_{sm} \Delta\omega_m = P_m - P_e. \quad (2.31)$$

It is a common practice to express the angular momentum of the rotor  $J\omega_{sm}$  in terms of a normalized inertia constant. The inertia constant is given by symbol H defined as the stored kinetic energy in mega joules at synchronous speed divided by the machine rating  $S_n$  in megavolt-ampere, where

$$H = \frac{0.5J\omega_{sm}^2}{S_n}. \quad (2.32)$$

Damping of the rotor by mechanical losses is small and can be neglected for all practical considerations. In the transient state, the air-gap flux which rotates at the synchronous speed, penetrates the damper winding and induces an emf and current in them whenever the rotor speed  $\omega$  is different from the synchronous speed  $\omega_{sm}$ . This induced current produces a damping torque and hence the damping power which according to

Lenz's law tries to restore the synchronous speed of the rotor. The swing equation in terms of damping power is obtained by

$$J\omega_{sm} \frac{d\omega_m}{dt} = P_m - P_e - P_D. \quad (2.33)$$

If  $\Delta\omega_m > 0$ , then damping power will be negative i.e. effectively opposing the acceleration and if  $\Delta\omega_m < 0$ , then damping power will be positive and supporting the airgap power  $P_e$  in opposing the deceleration.

Synchronous generator rotor speed, under steady state conditions, is proportional to the frequency of the armature current and as a result the frequency of the terminal voltage. This is governed by the equation,

$$f_e = \left( \frac{\text{poles}}{2} \right) \cdot \frac{n}{60}. \quad (2.34)$$

$f_e$  = electrical frequency of the voltage generated by synchronous generator.

## 2.5.2 Virtual Synchronous Machine

The main aim of implementation of concept of virtual synchronous machine is to combine the dynamic characteristics of electromechanical synchronous machine with power electronic converters [17], [23] & [24]. The virtual synchronous machine implemented in this research work is based on a conventional swing equation representing the inertia and damping of traditional synchronous machine as discussed in previous section. In order to implement this swing equation, it needs to be linearized with respect to the speed. The acceleration of the inertia in swing equation is determined by the power balance according to the equation,

$$\frac{d\omega_{VSM}}{dt} = \frac{P_m}{T_m} - \frac{P_e}{T_m} - \frac{P_D}{T_m}. \quad (2.35)$$

In above equation,  $P_m$  is the virtual mechanical input power,  $P_e$  is the measured electrical power flowing from the VSM into the grid and  $P_D$  is the damping power, while  $T_m$  is the mechanical time constant (corresponds to  $2H$  in conventional synchronous machine) [17]. The mechanical speed  $\omega_{VSM}$  of the virtual synchronous machine is given by the integral of the power balance while the corresponding  $\theta_{VSM}$  is given by the integral of the speed. The figure 2.11 exhibit the block diagram representation of swing equation of virtual synchronous machine.

The damping power in virtual synchronous machine  $P_d$  is defined by the damping coefficient  $k_d$  and the difference between the speed of the rotor of virtual synchronous machine and the actual grid frequency and is very similar to the damping effect of conventional synchronous machine. Thus an estimate of actual grid frequency is needed for the implementation of virtual synchronous machine. As shown in figure 2.11, the frequency estimate from the grid is provided by PLL and is denoted by  $\omega_{PLL}$ .

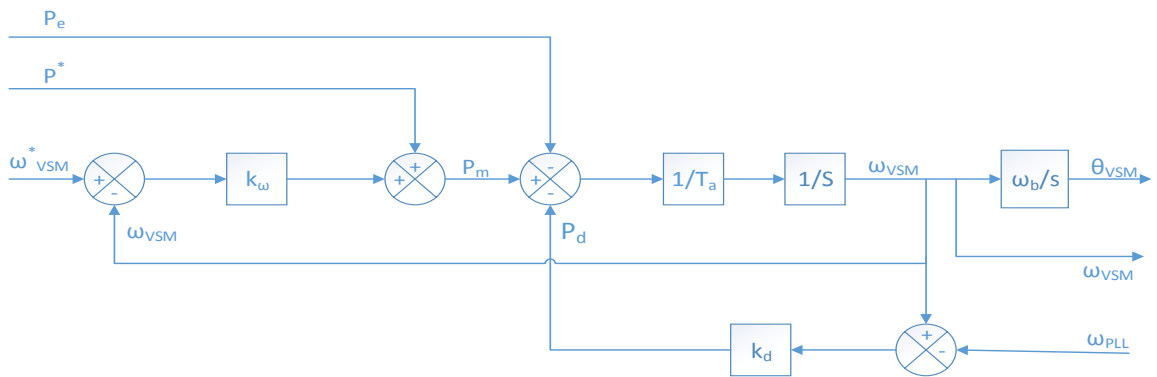


Figure 2.11 Virtual Synchronous Machine Swing Equation

The virtual mechanical input power  $P_m$  can be derived from power-frequency droop which is equivalent to the steady-state characteristics of the speed governor for conventional synchronous machine. This power-frequency droop is included in the swing

equation of virtual synchronous machine as shown in figure 2.11 and is characterized by the droop constant  $k_\omega$  acting on the difference between the frequency reference  $\omega^*_{VSM}$  and the actual speed  $\omega_{VSM}$ . Thus it is clear that input mechanical power  $P_m$  is the sum of the external power reference point  $P^*$  and the frequency droop effect.

For modelling the virtual synchronous machine in synchronous reference frame, the phase angle of the VSM in the grid connected mode should be constant under steady-state conditions and should correspond to the phase displacement between the virtual position of VSM internal voltage and the position of the grid voltage vector. Since only the deviation of the VSM speed from the actual grid frequency should be modelled to achieve this, a new set of variables representing the speed deviation  $\delta\omega_{VSM}$  and the corresponding phase angle difference  $\delta\theta_{VSM}$  is introduced. Thus the power balance of the virtual synchronous machine inertia and virtual synchronous machine phase displacement is defined by equations:

$$\frac{d\delta\omega_{VSM}}{dt} = \frac{P^*}{T_m} - \frac{P_e}{T_m} - \frac{k_d(\omega_{VSM} - \omega_{PLL})}{T_m} - \frac{k_\omega(\omega_{VSM} - \omega^*_{VSM})}{T_m} \text{ and} \quad (2.36)$$

$$\frac{d\delta\theta_{VSM}}{dt} = \delta\omega_{VSM} \cdot \omega_b. \quad (2.37)$$

Since the speed of virtual synchronous machine in steady state will become equal to the grid frequency  $\omega_{PLL}$ , the frequency deviation  $\delta\omega_{VSM}$  will return to zero under stable grid connected operation. The phase angle  $\theta_{VSM}$  will be used for the transformation between the rotating reference frame defined by the virtual synchronous machine inertia and the three phase signals. The figure 2.12 represents simulink model of virtual synchronous machine swing equation. The phase and frequency values obtained from VSM swing equation will be reference for microgrid islanded operation as well as for resynchronization



The most basic form of fuzzy control architecture is Mamdani architecture, which directly translates the crisp input from the plant data into a rule-based linguistic control strategy. As proposed by E.H. Mamdani, in absence of an explicit plant model and/or clear statement of control design objectives, informal knowledge of the operation of plant can be codified in terms of If-Then or condition-action rules and form the basis for a linguistic control strategy. The figure 2.13 shows the basic architecture of fuzzy control.

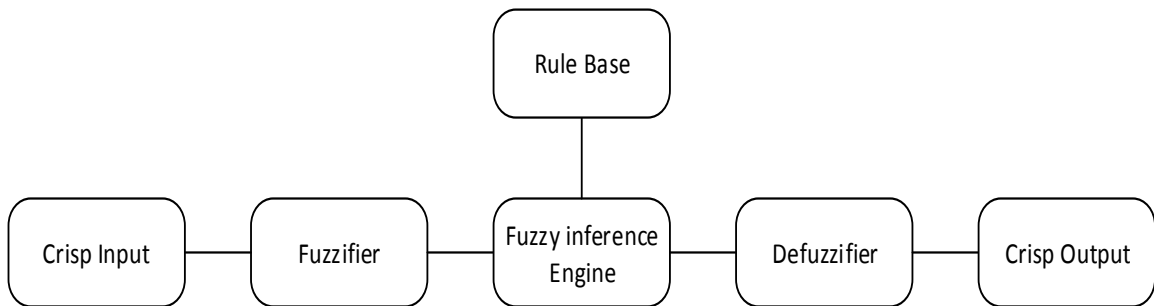


Figure 2.13 Architecture of Fuzzy Control

As we can observe in the fuzzy logic architecture block diagram above, the input and output of the fuzzy system are real valued numbers. Now in order to transform real valued numbers to fuzzy linguistic variable, we need to construct an interface between the fuzzy inference engine and the environment. The interfaces are the fuzzifier and defuzzifier [18].

- a) Fuzzifier: The fuzzifier is defined as a mapping of real valued point  $x \in U$  to a fuzzy set  $A \in U$  using the membership function. There are several types of membership functions to design a fuzzifier: 1) Triangular, 2) Trapezoidal, 3) Piecewise linear, 4) Gaussian, 5) Singleton. The membership function is a curve that define how an input value is mapped to a degree of membership between 0 and 1. The fuzzifier considered in this research work is a triangular fuzzifier. The fuzzifier maps  $x \in U$  into fuzzy set,  $A$  in  $U$ , which has triangular membership function represented by

$$\mu_A(x) = \{ (1 - \frac{|x_1 - x^*_1|}{b_1}) \dots \dots \dots (1 - \frac{|x_n - x^*_n|}{b_n}) \}, \quad (2.38)$$

if  $|x_i - x^*_i| \leq b_i, i = 1, 2, 3, 4, \dots, n$ , where  $b_i$  are positive parameters.

- b) Fuzzy Rule Base and Inference Engine: The fuzzy rule base consists of a set of fuzzy IF-Then rules. It is the heart of fuzzy system in the sense that all other components are used to implement these rules in a reasonable and efficient manner.

Specifically,

The fuzzy rule base comprises the following fuzzy IF-THEN rule

$$\text{Rule : IF } x_i \text{ is } A, \text{ THEN } y \text{ is } B, \quad (2.39)$$

where  $A_i$  and  $B$  are fuzzy sets and  $B \in V$ ,  $x$  and  $y$  are input and output linguistic variables of fuzzy system.

Fuzzy inference engine consists of fuzzy logic principles, which are used to combine the fuzzy IF-THEN rules in the fuzzy rule base into a mapping from a fuzzy set  $A$  in  $U$  to a fuzzy set  $B$  in  $V$ . There are two ways to infer with a set of rules: composition based inference and individual-rule based inference. Individual rule based fuzzy inference method is considered in this research work.

- c) Defuzzifier: The defuzzifier is defined as a mapping from fuzzy set  $B$  in  $V$  (which is output of fuzzy inference engine) to crisp value  $y \in V$ . Conceptually, task of defuzzifier is to specify point in  $V$  that best represents the point in  $B$ . There are several methods of defuzzifier, but the one considered in this work is center of gravity defuzzifier. The center of gravity defuzzifier specifies the  $y$  as the center of the area covered by the membership function of  $B$  i.e.

$$y = \frac{\int_v y \mu_B(y) dy}{\int_v \mu_B(y) dy}, \quad (2.40)$$

where  $\int_v$  is the conventional integral.

- d) Generic fuzzy control: The figure 2.14 shows the generic fuzzy control plant model.

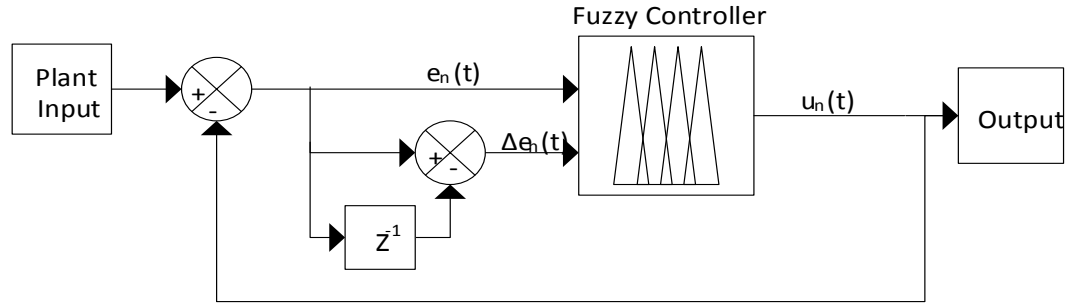


Figure 2.14 Generic Fuzzy Control Plant Model

We then proceed to develop a control strategy that maps the error  $e(t)$  into the control action  $u_n(t)$ . The fuzzy logic controller operates in discrete time steps of period  $T$  and maps value of error and rate of change of error, defined as,

$$e_n(t) = e(t) \text{ and} \quad (2.41)$$

$$\Delta e_n(t) = e(t) - e(t - T). \quad (2.42)$$

The output of the fuzzy logic controller is  $u_n(t)$  is obtained by defuzzifying the following sample rule from rule base:

IF  $e_n(t)$  is P and  $\Delta e_n(t)$  is N THEN  $u_n(t)$  is Z, where P is positive, N is negative and Z is zero.

Similarly, fuzzy control technique is proposed and implemented for V-F control of voltage source converter of energy storage system in Microgrid which is explained in detail in next chapter.

# **CHAPTER 3 MODELING AND CONTROL OF MICROGRID**

This chapter mainly discuss about modelling, selection and sizing of microgrid components and also the decentralized control of voltage, frequency, active and reactive power in power electronic converter based DER and energy storage system in microgrid. The main advantage of power electronic converters is that it enables implementation of advanced control techniques to improve the performance of electric power grid. The design of control system for power electronic converter in microgrid depends mainly on two criteria: 1) Type of DER and 2) Mode of operation of Microgrid. The new virtual synchronous machine based fuzzy V-F control strategy with cascade synchronization controller, proposed in this research work for energy storage system, will aid stable operation of microgrid in both grid-connected and islanded mode. The proposed control methodology in this research work coordinates PV generation unit active/reactive power control through maximum power point tracking in grid connected mode, voltage/frequency control through battery storage system in islanded mode and seamless transition of microgrid from both the modes of operation.

## **3.1 Modeling of Microgrid Components**

The system test model to validate the performance of proposed controller is explained in this chapter. The test model of microgrid consists of PV generation unit and battery energy storage unit to feed the local loads, which is modeled based on the hourly load profile. The PV generation unit and battery energy storage system is connected to the 3 phase AC grid at PCC through voltage source converter, LC filter and transformer at

PCC. The voltage at PCC is 4.16 kV (ph-ph rms). The average model for the voltage source converter is adopted for faster simulation and reduce data processing efforts.

### **3.1.1 Modeling of Microgrid Load Profile**

As we all know that electrical loads display non-linearity or random variability. Thus it is very important to add non linearity to the load data taken into consideration for simulation of Microgrid Model. Non linearity in the electric load is due to the aggregation of different types of commercial, domestic and industrial users. It is very difficult to forecast the behavior of different user over wide span of time. The factors that affect the load profile are user habits, atmospheric conditions, seasonal changes, emergency situations, rate of growth of population etc. Hence average of daily load profile is taken into consideration for forecast and calculation of power flow in Microgrid.

The Load profile is constructed using HOMER Microgrid Analysis tool for this work. The load profile constructed is for University of Houston, Houston, TX, as discussed in section 1 of this chapter. The figure 3.1 and table 3.1 depicts the daily load profile, average and peak values of the load and graphical representation of daily and seasonal load profile over the entire year.

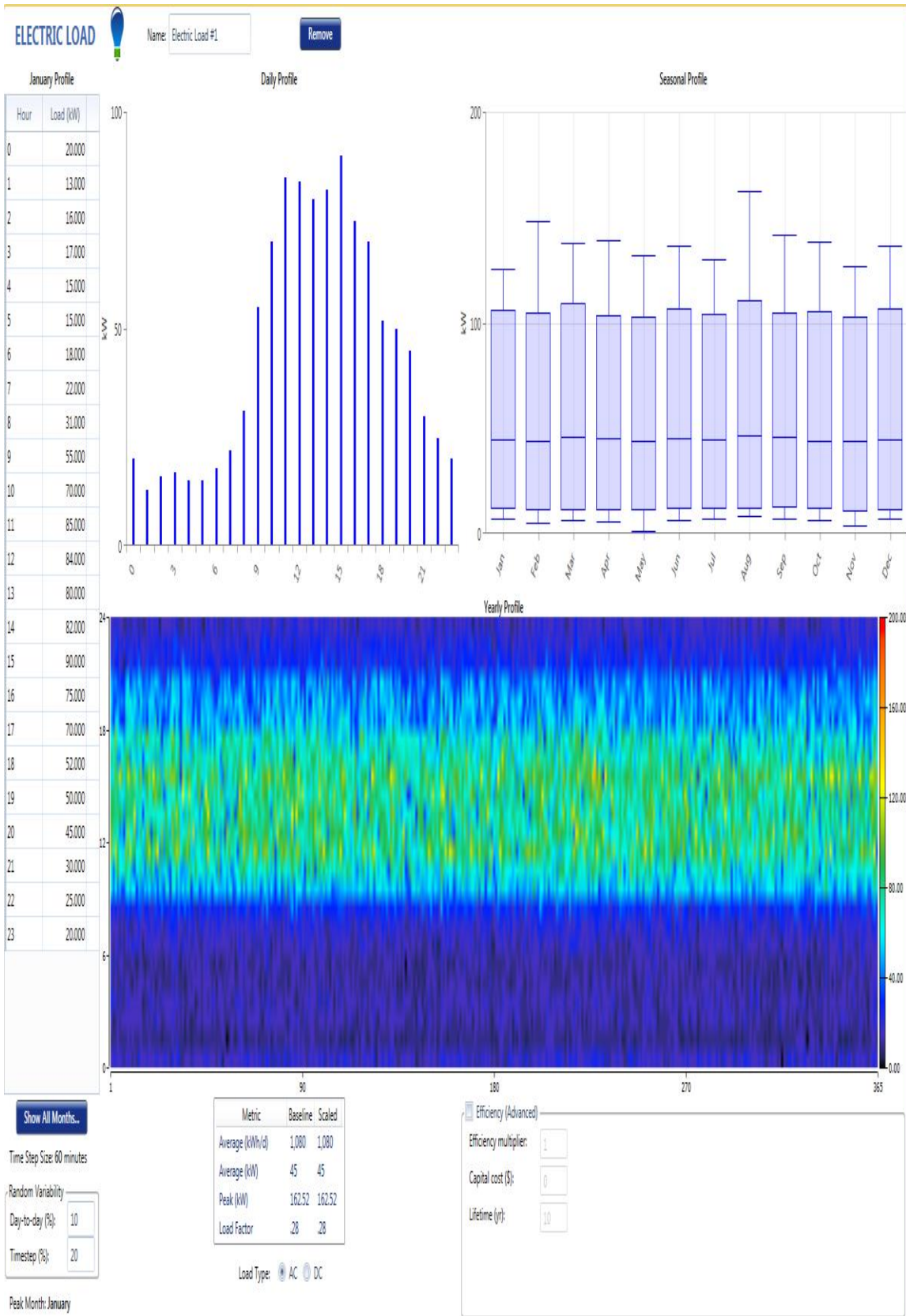


Figure 3.1 HOMER Load Profile Evaluation

Table 3.1 Yearly Load Data (in kW)

Hour	January	February	March	April	May	June	July	August	September	October	November	December
0	20	20	20	20	20	20	20	20	20	20	20	20
1	13	13	13	13	13	13	13	13	13	13	13	13
2	16	16	16	16	16	16	16	16	16	16	16	16
3	17	17	17	17	17	17	17	17	17	17	17	17
4	15	15	15	15	15	15	15	15	15	15	15	15
5	15	15	15	15	15	15	15	15	15	15	15	15
6	18	18	18	18	18	18	18	18	18	18	18	18
7	22	22	22	22	22	22	22	22	22	22	22	22
8	31	31	31	31	31	31	31	31	31	31	31	31
9	55	55	55	55	55	55	55	55	55	55	55	55
10	70	70	70	70	70	70	70	70	70	70	70	70
11	85	85	85	85	85	85	85	85	85	85	85	85
12	84	84	84	84	84	84	84	84	84	84	84	84
13	80	80	80	80	80	80	80	80	80	80	80	80
14	82	82	82	82	82	82	82	82	82	82	82	82
15	90	90	90	90	90	90	90	90	90	90	90	90
16	75	75	75	75	75	75	75	75	75	75	75	75
17	70	70	70	70	70	70	70	70	70	70	70	70
18	52	52	52	52	52	52	52	52	52	52	52	52
19	50	50	50	50	50	50	50	50	50	50	50	50
20	45	45	45	45	45	45	45	45	45	45	45	45
21	30	30	30	30	30	30	30	30	30	30	30	30
22	25	25	25	25	25	25	25	25	25	25	25	25
23	20	20	20	20	20	20	20	20	20	20	20	20

### 3.1.2 Modeling of PV Array

The selection and sizing of PV generation unit is based on the availability of solar irradiance over an entire year, type of solar cell and its efficiency, peak demand during certain hours of the day and economic analysis. The HOMER analysis tool performs the sensitivity analysis considering all the above mentioned criteria as well as the load profile evaluation and suggest the capacity required for PV generation unit, which is 400 kW. The PV array model considered for Simulation in MATLAB is SunPower SPR-305E-WHT-D. The 400 kW SunPower SPR-305E-WHT-DPV array consists of 264 strings of 5 series

connected modules connected in parallel. Each module consists of 96 series connected cells with open circuit voltage ( $V_{oc}$ ) 64.2 V and short circuit current ( $I_{sc}$ ) 5.9 A. The figure 3.2 shows simulink equivalent model of PV array module. The voltage and current at maximum power point is  $V_{MPP} = 54.7 V$  and  $I_{MPP} = 5.58 A$ . The figure 3.3 and 3.4 shows P-V and I-V characteristics of PV array SPR-305E-WHT-D.

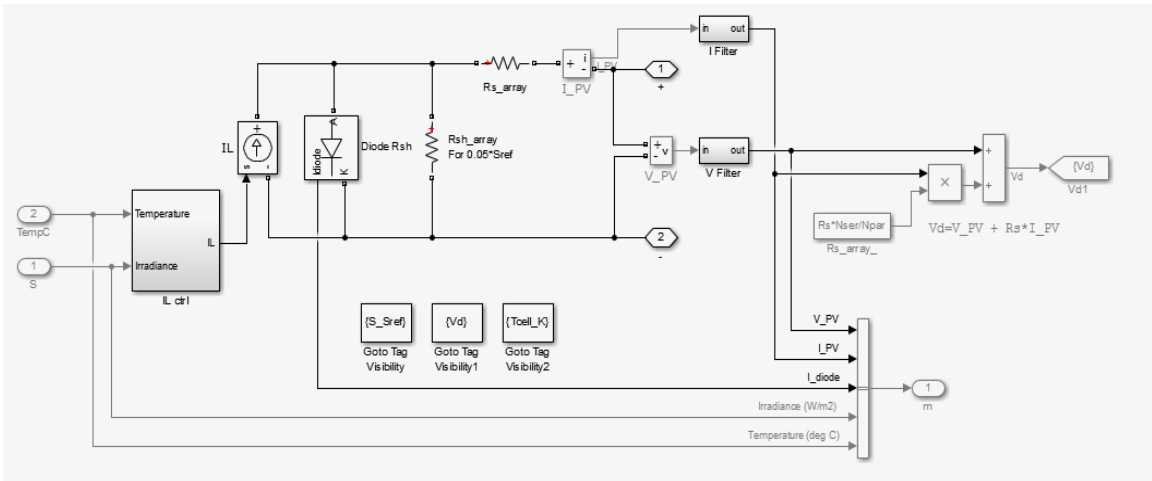


Figure 3.2 Simulink Equivalent Model of PV Array

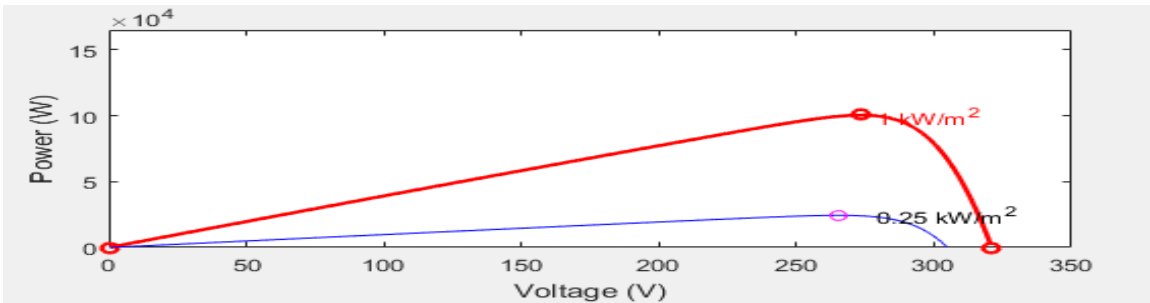


Figure 3.3 P-V Characteristic of PV Array SPR-305E-WHT-D

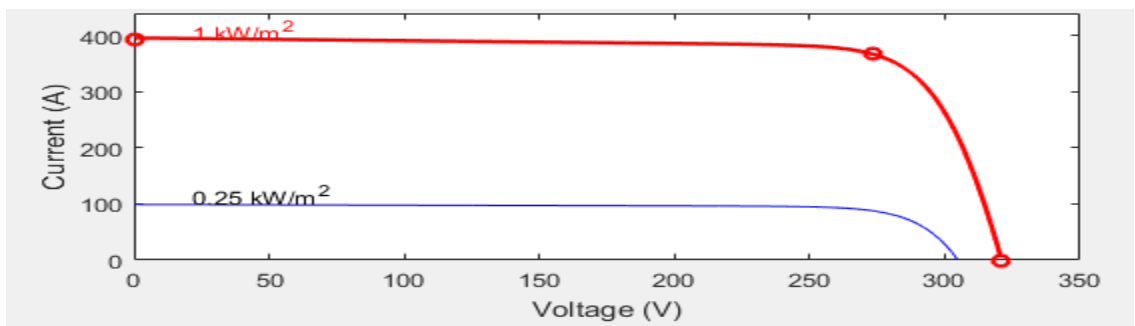


Figure 3.4 I-V Characteristic of PV Array SPR-305E-WHT-D

The PV generation unit is integrated to a utility grid at PCC via DC/DC boost converter and DC/AC converter which is controlled by P-Q control in both grid connected and islanded mode.

### 3.1.3 Modeling of Battery Energy Storage System (BESS)

PV generation units are not dispatchable because of their intermittent characteristics. But energy storage system can be an added advantage to make it dispatchable, either by storing surplus power or by delivering it to the grid during the power deficit [8]. Power dispatch curve depicts the mismatch between the demand and generation over the time interval of one hour/60 minutes. Normally load dispatch center considers 15 minute time period for dispatch and generation dispatch is scheduled for 30 minute time period, but for smooth calculation the time period considered here is of 1 hour.

Let  $P_g$  be the power generated by solar array,  $P_d$  be the demand side power or load that needs to be dispatched by the generator over certain defined time interval  $\Delta t$  and  $P_{mis}$  be the power mismatch in the system. The average charge/discharge power for the battery energy storage system per day in kWh/day be  $P_{bat}$ .

$$P_{mis}(t) = P_g(t) - P_d(t). \quad (3.1)$$

Now  $P_{bat}$  is calculated from power mismatch i.e. surplus or deficit power in the grid.

$$P_{bat}(kWh) = \max\{\sum_1^N P_{mis} \times \Delta t\}, \quad (3.2)$$

where N is the number of days in one year.

The table 3.2 and table 3.3 represents power mismatch, peak generation hours and peak as well as off-peak demand data for the month of August and December.

Table 3.2 Power Dispatch (Average) for Month of August

Power Dispatch (August 21 2016)				
Sr. No.	PV generation (kW)	Load (kW)	Power Mismatch (kW)	Hour of the Day
1	0	20	-20	12:00 AM
2	0	13	-13	1:00 AM
3	0	16	-16	2:00 AM
4	0	17	-17	3:00 AM
5	0	15	-15	4:00 AM
6	0	15	-15	5:00 AM
7	0	18	-18	6:00 AM
8	16.4	22	-5.6	7:00 AM
9	67.5	31	36.5	8:00 AM
10	133.63	55	78.63	9:00 AM
11	220.99	70	150.99	10:00 AM
12	303.96	85	218.96	11:00 AM
13	347.95	84	263.95	12:00 PM
14	350.74	80	270.74	1:00 PM
15	357.23	82	275.23	2:00 PM
16	316.5	90	226.5	3:00 PM
17	257.45	75	182.45	4:00 PM
18	167.6	70	97.6	5:00 PM
19	62.74	52	10.74	6:00 PM
20	11.1	50	-38.9	7:00 PM
21	0	45	-45	8:00 PM
22	0	30	-30	9:00 PM
23	0	25	-25	10:00 PM
24	0	20	-20	11:00 PM

Table 3.3 Power Dispatch (Average) for Month of December

Power Dispatch (December 4 2016)				
Sr. No.	PV generation (kW)	Load (kW)	Power Mismatch (kW)	Hour of the Day
1	0	20	-20	12:00 AM
2	0	13	-13	1:00 AM
3	0	16	-16	2:00 AM
4	0	17	-17	3:00 AM
5	0	15	-15	4:00 AM
6	0	15	-15	5:00 AM
7	0	18	-18	6:00 AM
8	0	22	-22	7:00 AM
9	1.52	31	-29.48	8:00 AM
10	16.74	55	-38.26	9:00 AM
11	28.49	70	-41.51	10:00 AM
12	18.98	85	-66.02	11:00 AM
13	28.95	84	-55.05	12:00 PM
14	21.55	80	-58.45	1:00 PM
15	22.65	82	-59.35	2:00 PM
16	9.17	90	-80.83	3:00 PM
17	28.96	75	-46.04	4:00 PM
18	15.46	70	-54.54	5:00 PM
19	0	52	-52	6:00 PM
20	0	50	-50	7:00 PM
21	0	45	-45	8:00 PM
22	0	30	-30	9:00 PM
23	0	25	-25	10:00 PM
24	0	20	-20	11:00 PM

The factors that need to be considered for selection and sizing of battery are depth of discharge (%DOD), days of autonomy (D), and battery ageing. Day of autonomy (D) is nothing but the dispatch capacity of the battery as a back-up without charging. The operating temperatures and ageing also affect the performance of battery energy storage system. The temperature correction factor for an average operating temperature is found to be 0.964. The ageing characteristics of the battery is considered by assuming an ageing factor of 15%. The final correction factor for sizing of battery energy storage system is calculated by,

$$\begin{aligned} \text{Correction factor for Temperature and Age effect} &= (0.964 \times 1.15) = 1.108 \\ &\approx 110\%. \end{aligned} \quad (3.3)$$

Now based on the values obtained for  $P_{bat}$  from table 3.2 and equation 3.3, the maximum required battery capacity can be calculated by,

$$P_{bat(max)} = \frac{110 \times P_{bat} \left( \frac{kWh}{day} \right) \times D}{\%DOD} \quad (3.4)$$

From equation 3.4 the calculated value for  $P_{bat(max)}$  is 2168.22 kWh.

When the system under study is evaluated on HOMER microgrid analysis tool, the optimized design value obtained for nominal capacity of battery energy storage system, based on the load profile is 2000 kWh. This result is very similar to the calculated value of 2168.22 kWh. The figure 3.5 shows the optimization results of HOMER microgrid analysis tool simulation for battery energy storage system sizing and selection.

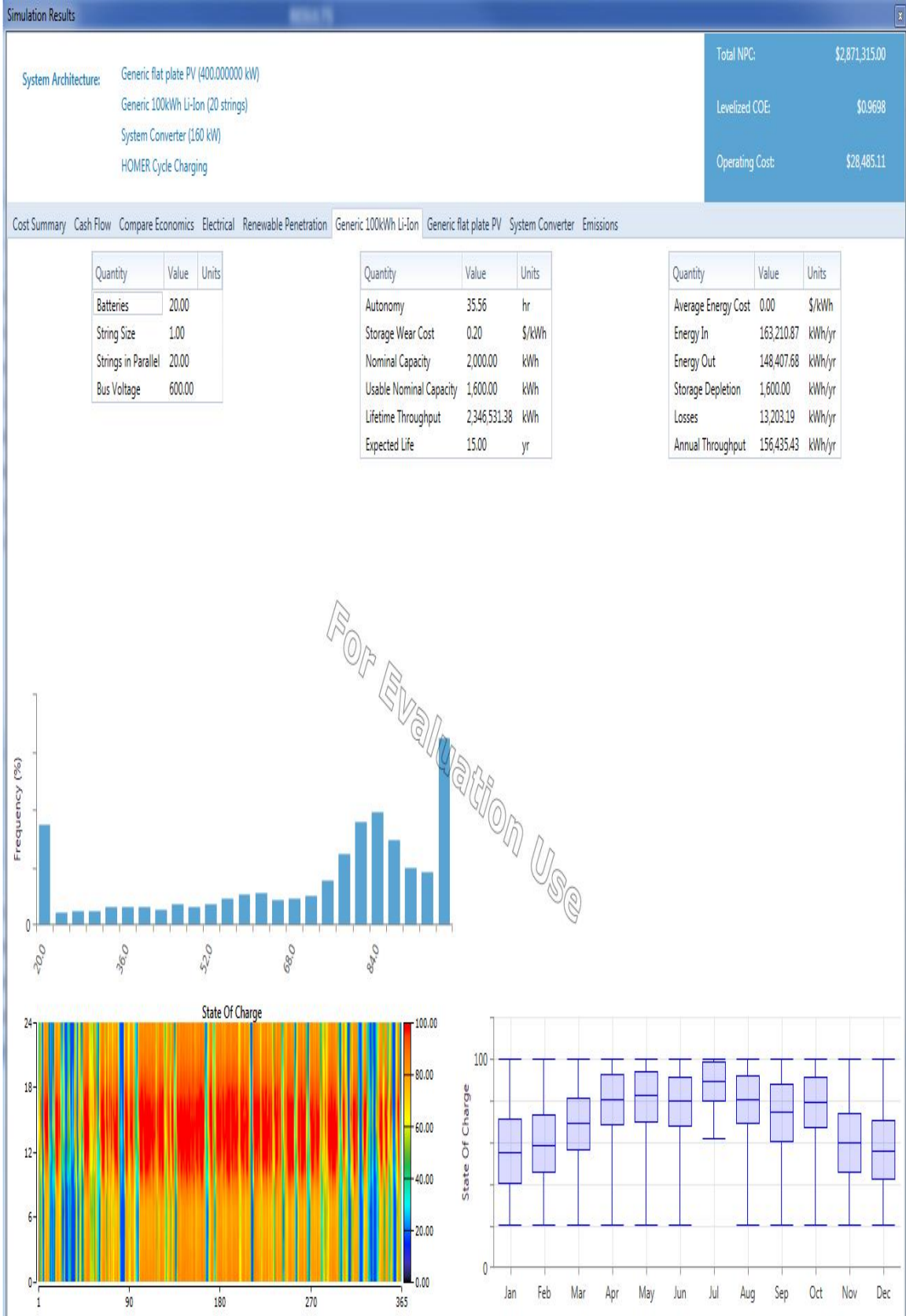


Figure 3.5 Simulation Tool Result for Battery Sizing and Selection

The battery size obtained by above calculations will be able to feed the load for about two days autonomously as a back-up without any charging. The battery rating in Ah can be obtained by (watt-hour/battery voltage). In this case the capacity of battery in Ah will be  $2000000 \text{ Wh} / 400 \text{ V} = 5000 \text{ Ah}$  (where 400V is DC bus voltage). Now the ratio of maximum battery storage system capacity to individual battery capacity will yield the number of modules to be connected in parallel to obtain the desired output. The data for individual battery module can be obtained from TESVOLT TLC 120 battery system datasheet [9]. Now based on the datasheet, the maximum output power from each battery module is 98kWh, which means 20 such modules need to be connected in parallel to obtain total output of 2000kWh. The battery energy storage system will be connected to the grid through bidirectional DC-DC buck-boost converter and DC/AC inverter which is controlled by P-Q control in grid connected mode and V-F control in islanded mode. The figure 3.6 shows a simulink model of microgrid test system.

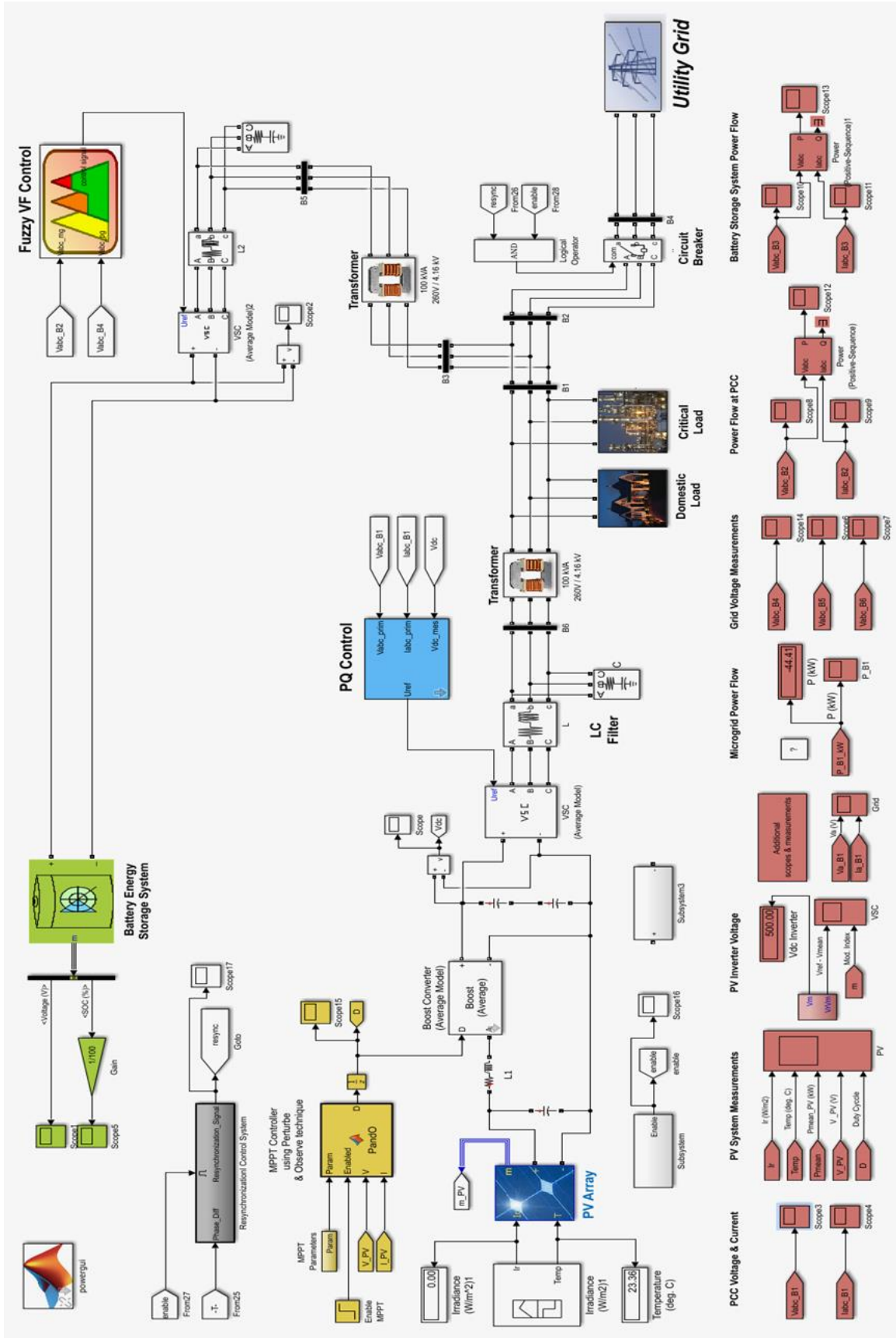


Figure 3.6 Simulink Model of Microgrid Test System

## 3.2 Control of Microgrid in Grid-Connected Mode (P-Q Control)

The microgrid is connected to the main utility grid through voltage source converters and circuit breakers at point of common coupling (PCC). When microgrid is connected to the grid, the voltage and frequency at PCC is controlled by the grid and DERs have to maintain active and reactive power flow to feed the local loads, thus acting as P-Q bus. A control technique for active and reactive power flow from PV generation unit is developed with two control loops i.e. inner and outer feedback control loop [14].

### 3.2.1 Inner Control Loop

The inner control loop is also called the current control loop or current regulator, since it regulates the current flowing through series inductor L of LC low pass filter. The current across the inductor can be calculated from the voltage drop across inductive reactance. The voltage drop is calculate by equation

$$V_{prim}^{abc} - V_{conv}^{abc} = Ri_{abc} + L \frac{di_{abc}}{dt}, \quad (3.5)$$

where  $V_{prim}^{abc}$ (3-phase) is the voltage at PCC and  $V_{conv}^{abc}$ (3-phase) is the voltage on the AC side of the converter and  $i_{abc}$  is the line current through the inductor L. Now in order to simplify the calculations for control, three phase quantities would be transformed into single rotating reference frame which is called dq0 or park transformation.

If the equation 3.5 is transformed to dq0, then we get the following two equations:

$$V_{prim,d} - V_{conv,d} = Ri_d + L \frac{di_d}{dt} - \omega Li_q \text{ and} \quad (3.6)$$

$$V_{prim,q} - V_{conv,q} = Ri_q + L \frac{di_q}{dt} + \omega Li_d, \quad (3.7)$$

where  $V_{prim,d}$  and  $V_{prim,q}$  are direct and quadrature axis component of voltage at PCC and  $V_{conv,d}$  and  $V_{conv,q}$  are components of converter voltage. Similarly,  $i_d$  and  $i_q$  are direct and

quadrature components of current through the inductor.

In order to generate reference signals to control the inverter output, PI controller is designed

as

$$V_{conv,d} = V_{prim,d} - [k_p(i_d^* - i_d) + k_i \int (i_d^* - i_d) dt] + \omega L i_q \quad (3.8)$$

$$V_{conv,q} = V_{prim,q} - [k_p(i_q^* - i_q) + k_i \int (i_q^* - i_q) dt] - \omega L i_d, \quad (3.9)$$

where  $k_p$  and  $k_i$  are proportional and integral gain of the controller.

The block diagram of the inner control loop is represented in figure 3.7.

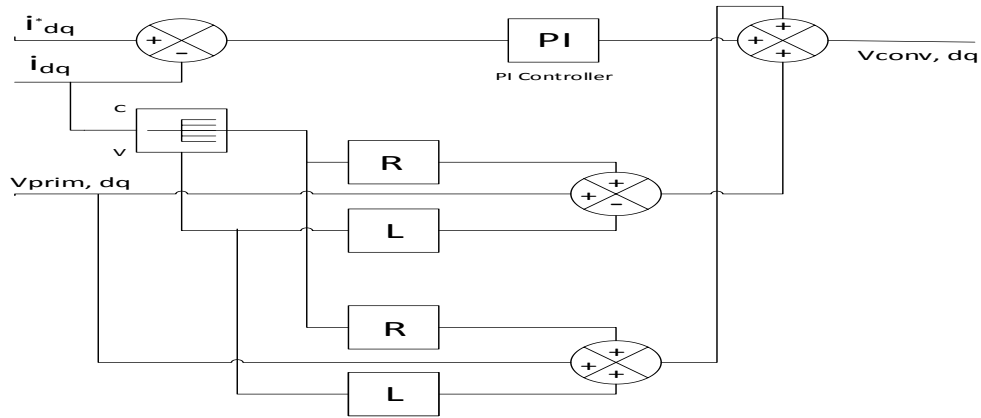


Figure 3.7 Inner Control Loop for P-Q Control (PV Array)

The simulink implementation of inner control loop discussed above is shown in figure 3.8.

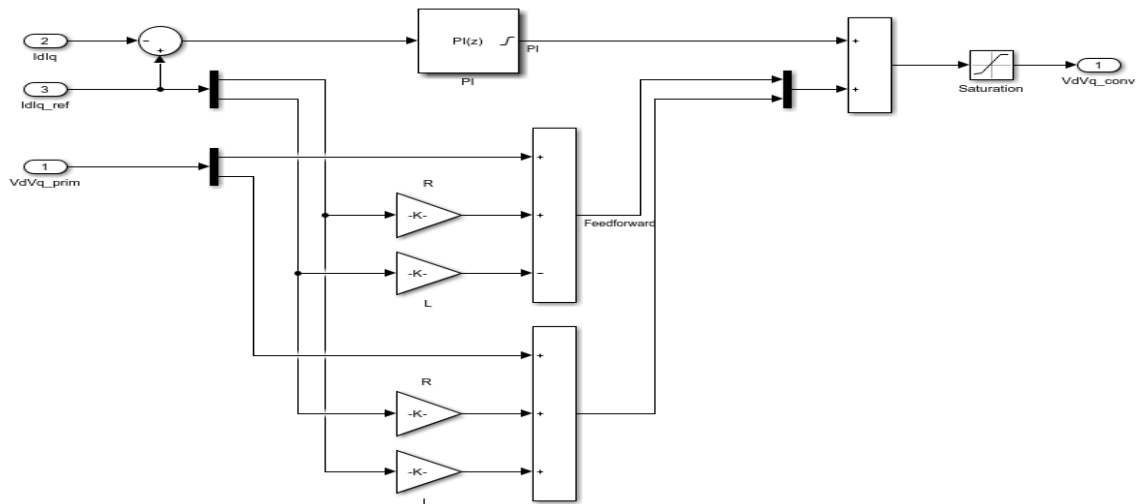


Figure 3.8 Simulink Model of Inner Control Loop of P-Q Control for PV Generation Unit

### 3.2.2 Outer Control Loop

The PV generation unit generates peak power at particular value of voltage and current. As discussed in chapter 3, MPPT control tries to draw the maximum power from PV generation unit by controlling either the voltage or current at input terminal of voltage source converter. In this research work, the DC voltage at the input terminal of voltage source converter is regulated by controlling the output current of PV generation unit with PI controller. This forms the outer control loop, also called as DC voltage regulator. Now according to power conservation theorem and considering the system to be lossless, power on the AC and DC side will be equal i.e.  $P_{AC} = P_{DC}$ . Hence,

$$V_{DC} \cdot I_{DC} = \frac{3}{2} V_{prim,d} \cdot i_d. \quad (3.10)$$

As we discussed above, the DC voltage can be regulated by PI controller, which is represented by

$$i_d^* = \left( k_p + \frac{k_i}{s} \right) \cdot (V_{DC}^* - V_{DC}), \quad (3.11)$$

where,  $V_{DC}^*$  is reference value of DC voltage.

The figure 3.9 represents the block diagram of outer control loop equation of P-Q control.

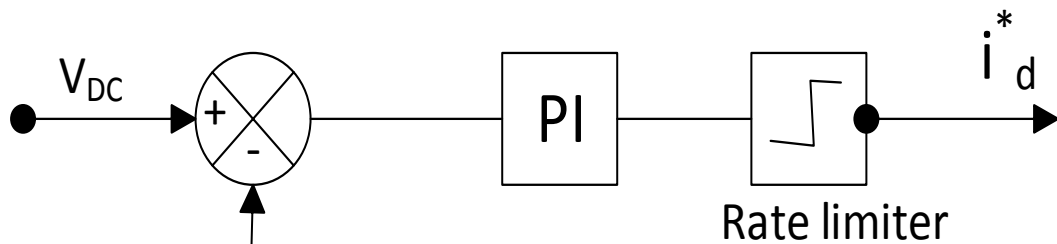


Figure 3.9 Outer Control Loop for P-Q Control

Thus by controlling direct-axis component of the inductor current, we can balance the flow of active power on DC and AC side. The reactive power flow will be controlled by quadrature-axis component of inductor current i.e.  $i_q$ . In this research work, there is no need of power factor control, since it is assumed to be lossless system and hence reactive power reference can be assumed to be zero. Based on this assumption, the quadrature-axis current reference will be zero too. Both direct-axis and quadrature-axis current reference will be fed to the inner control loop as shown in simulink block diagram in figure 3.10.

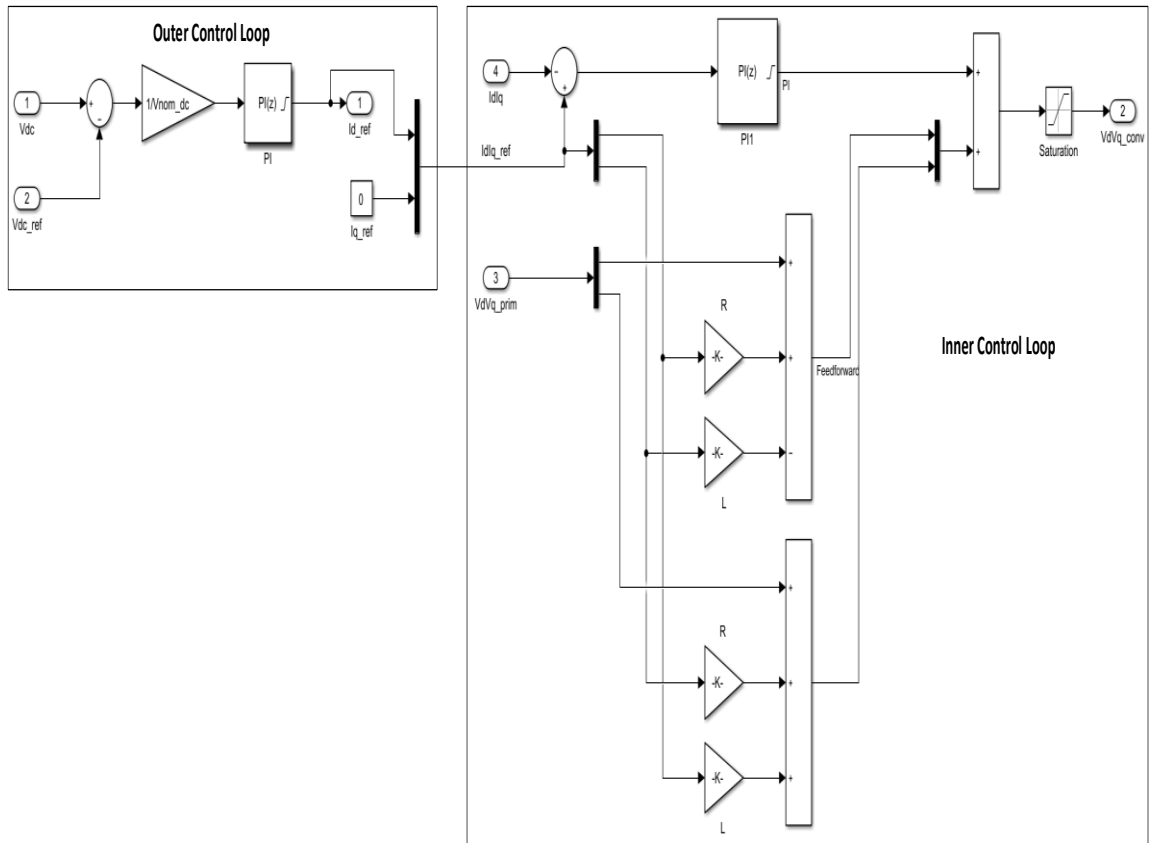


Figure 3.10 Simulink Block Diagram of P-Q Control for PV Generation Unit

In grid connected mode, the proposed control strategy for VSC of battery storage system will regulate the AC voltage error and balance the active power flow while charging or discharging of the battery. The proposed controller will be discussed in detail in next section.

### **3.3 Control of Microgrid in Islanded Mode (V-F Control)**

When microgrid is connected to the active utility grid, the microgrid receives the voltage and frequency reference from the grid. Thus VSC of DERs in microgrid operates in P-Q control mode to track the maximum power and feed the local loads efficiently. The operation of microgrid in islanded mode needs to regulate the voltage and frequency independently within the desired limit for stable operation, along with P-Q control. In this research work, DERs taken into consideration for microgrid modelling is PV generation unit and battery energy storage system. The PV generation unit have intermittent characteristics, and hence VSC of PV cannot operate in V-F control mode. The VSC of battery energy storage system operates in V-F control mode, since output of battery system (performance of battery storage system is discussed in previous chapter of this research work) is constant as compared to PV generation unit. The rating of battery storage system designed in this research work is such that it can feed the local loads (based on the load profile modeled in previous section) in islanded mode for up to two days without any backup, when there is no output power from PV generation unit, while regulating the voltage and frequency of the microgrid within the desired range.

The virtual synchronous machine based fuzzy V-F control technique for VSC of battery energy storage system coordinated with microgrid central controller proposed in this work can operate efficiently under following different scenarios:

- 1) Seamless transition of Microgrid from grid-connected mode to islanded mode.
- 2) Balance voltage and frequency of microgrid in islanded mode when there is low or no power generation by PV, through active power dispatch from the battery energy storage system to the local loads.

- 3) When the power supply from the PV does not meet the demand during islanded operation, and if battery state of charge is below the desired limit, then central controller will send a signal to shed non-critical loads, so that VSC of energy storage system can maintain the grid frequency and voltage for longer period.
- 4) If microgrid is operating in islanded mode over a longer period, then microgrid voltage, frequency, and phase will be different from the utility grid at PCC. The VSM based proposed control strategy will resynchronize the microgrid parameters with the main utility grid before reconnection. Hence we will have seamless transition of microgrid from islanded mode to grid connected mode.

The following sections will explain the proposed control strategy in detail.

### **3.3.1 Virtual Synchronous Machine based Fuzzy V-F Control**

The proposed fuzzy logic controller for V-F control of voltage source converter of battery energy storage system in islanded mode is of Mamdani type and is simulated in MATLAB/Simulink environment. The proposed fuzzy controller maps the voltage error into control signal for voltage source converter of battery storage system to regulate the voltage of an islanded microgrid. It is very difficult to map the error of all the three phase together. Hence the three-phase voltage  $V_{abc}$  is first transformed to dq0 components by park transformation. Two different fuzzy controllers are implemented, one for direct-axis voltage and other for quadrature-axis voltage. The fuzzy controller operates in discrete time steps of  $T_{s\_Power} = 5 \times 10^{-5}s$  and maps the value of voltage error and change of voltage error given by the equations

$$e(t) = V_{dq} - V_{dq,ref} \text{ and} \tag{3.12}$$

$$\Delta e(t) = e(t) - e(t - T_{s_{power}}), \quad (3.13)$$

where  $V_{dq}$  is dq0 transformed voltage vectors of Microgrid bus voltage at PCC in islanded mode,  $V_{dq,ref}$  is the reference voltage vector obtained fed by virtual synchronous machine and  $e(t)$  and  $\Delta e(t)$  are linguistic variables of fuzzy set.

The values of voltage error and change of voltage error obtained are real integers and needs to be transformed to linguistic value in fuzzy set through fuzzifier membership function. The linguistic values for an error can be defined by considering that error can be big, medium, and small or zero and can also be either positive or negative. Thus linguistic values for input linguistic variable will be,

$e(t) = \{NB, NM, NS, Z, PS, PM, PB\}$  and  $\Delta e(t) = \{NB, NM, NS, Z, PS, PM, PB\}$ , where NB = Negative Big, NM = Negative Medium, NS = Negative Small, Z = Zero, PS = Positive Small, PM = Positive Medium, and PB = Positive big. Each linguistic value is represented in form of membership function. Triangular membership function is taken into consideration to design the fuzzy sets. The figure 3.11 shows the triangular membership functions and fuzzy sets implemented to map the  $V_{dq}$  voltage error and change of error.

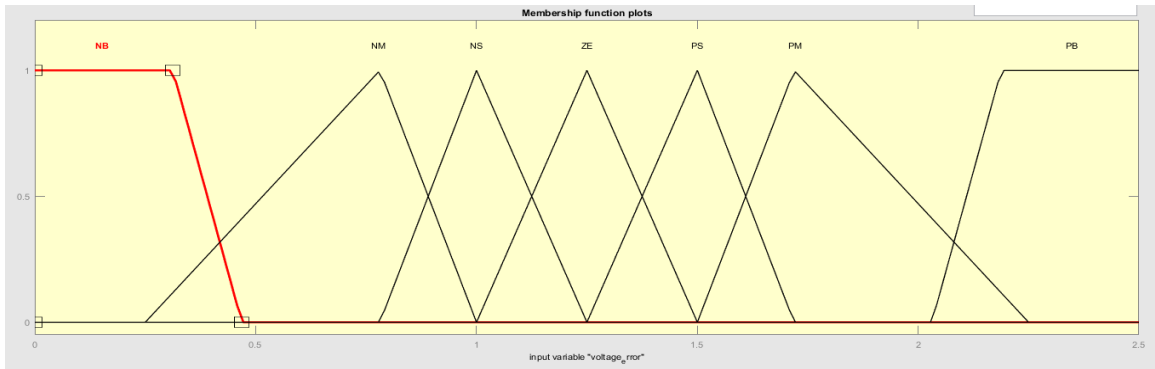


Figure 3.11 (a) Membership Function Plot for Input  $V_d$  Voltage Error

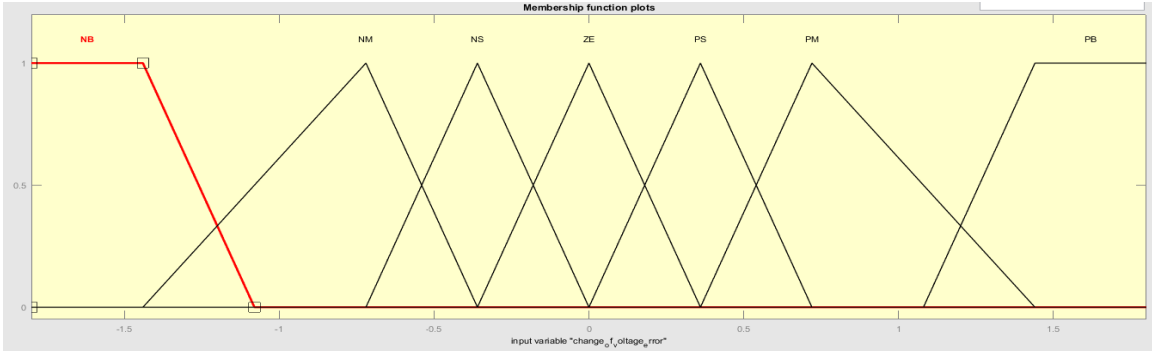


Figure 3.11 (b) Membership Function Plot for Input  $V_d$  Change of Voltage Error

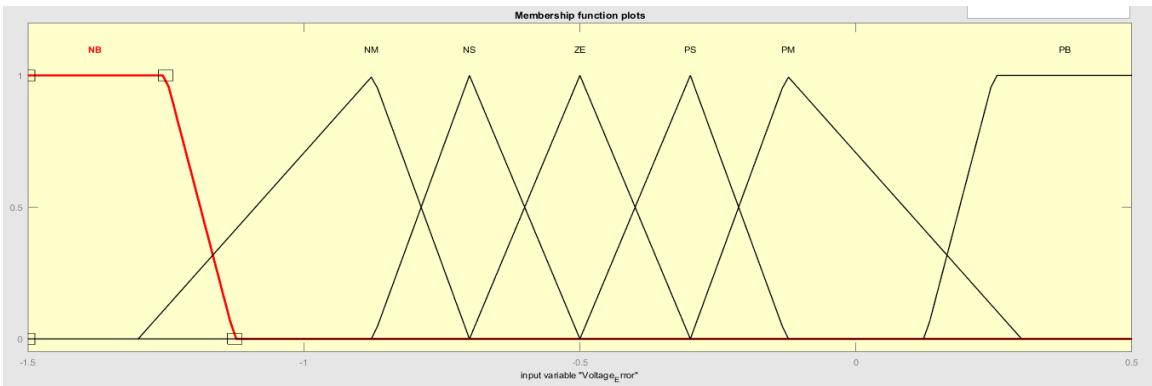


Figure 3.11 (c) Membership Function Plot for Input  $V_q$  Voltage Error

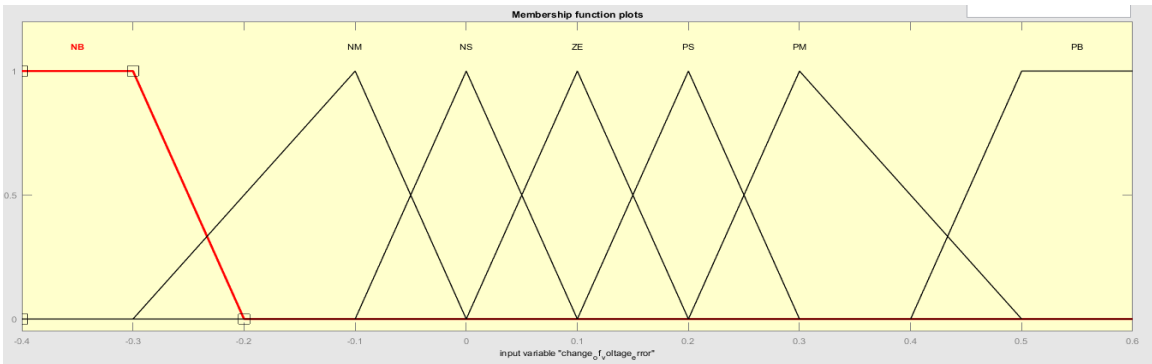


Figure 3.11 (d) Membership Function Plot for Input  $V_q$  Change of Voltage Error

After mapping the input error and change of error values to fuzzy set, they infer with fuzzy rule base in fuzzy inference engine. The table 3.4 shows the fuzzy rule base designed for V-F control.

Table 3.4 Fuzzy V-F Control Rule Base

Output $u(t)$		Change of Error $\Delta e(t)$						
		NB	NM	NS	Z	PS	PM	PB
Error $e(t)$	NB	Z	Z	Z	PB	PB	PB	PB
	NM	Z	Z	Z	PM	PM	PM	PM
	NS	Z	Z	Z	PS	PS	PS	PS
	Z	PS	Z	Z	Z	Z	Z	NS
	PS	NS	NS	NS	NS	Z	Z	Z
	PM	NM	NM	NM	NM	Z	Z	Z
	PB	NB	NB	NB	NB	Z	Z	Z

The output of the fuzzy inference engine is in fuzzy set. The fuzzy set needs to be transformed to crisp set or to real values integer to send it to the voltage source converter. The defuzzifier is used to map the fuzzy set into crisp set. The type of defuzzifier used here is center of gravity. The figure 3.12 shows the block diagram of fuzzy controller model for V-F control of microgrid in islanded mode of operation.

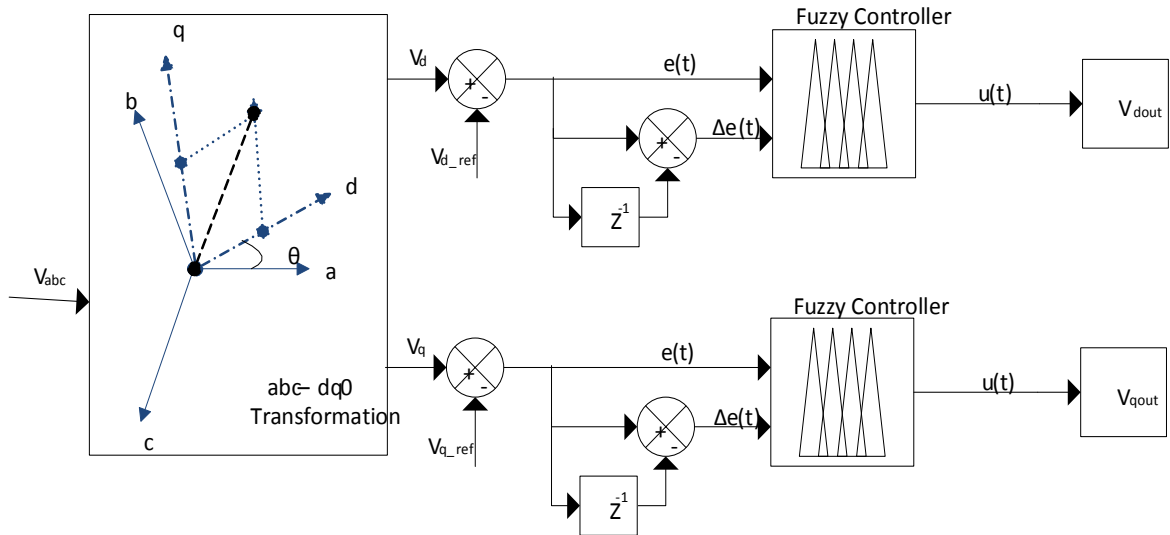


Figure 3.12 Fuzzy V-F Control Implementation Block Diagram

The crisp value of output direct and quadrature axis voltage is then transformed to three phase voltage  $V_{abc}$  through inverse park transformation. The reference value of frequency for inverse park transformation is obtained from virtual synchronous machine swing

equation. The output control signal is then fed to the voltage source converter of battery energy storage system to maintain voltage and frequency of islanded microgrid. The performance of the controller is validated for seamless transition of microgrid from grid connected mode to islanded mode and for stable performance of microgrid in islanded mode through the simulation results.

The only issue that prevails now is seamless transition of microgrid from islanded mode to grid connected mode. While islanded operation of the microgrid, voltage, phase and frequency reference is obtained from virtual synchronous machine, which can be different from utility grid voltage, phase and frequency at PCC. Thus it is important to synchronize them before reconnection of microgrid to the main utility grid in order to prevent high inrush current at PCC and damage the equipment. A synchronization controller is proposed in cascade with fuzzy V-F control and it enables only during reconnection of microgrid with the main grid.

### **3.3.1.1 Synchronization Controller**

The synchronization controller is enabled only if it receives enable signal from the microgrid central controller. The synchronization controller tracks the frequency and phase angle at PCC on both sides of the circuit breaker through PLL for microgrid and main utility grid. The input of synchronization controller is frequency difference  $\Delta\omega$  and phase angle difference  $\Delta\theta$  between the microgrid and main utility grid. The output of the controller will be incremental frequency reference  $\Delta\omega^*_{VSM}$  to the internal frequency  $\omega^*_{VSM}$  of virtual synchronous machine inertia equation and is generated by integral controller (I) instead of PI controller to ensure smooth and steady change in value of frequency without any overshoot. This can be explained by the equation,

$$\omega^*_{VSM} = \omega^*_{VSM} + \Delta\omega^*_{VSM}. \quad (3.14)$$

The integral controller I is disabled and incremental frequency reference  $\Delta\omega^*_{VSM}$  is set to zero when synchronization controller is not enabled. The figure 3.13 shows the block diagram of synchronization controller.

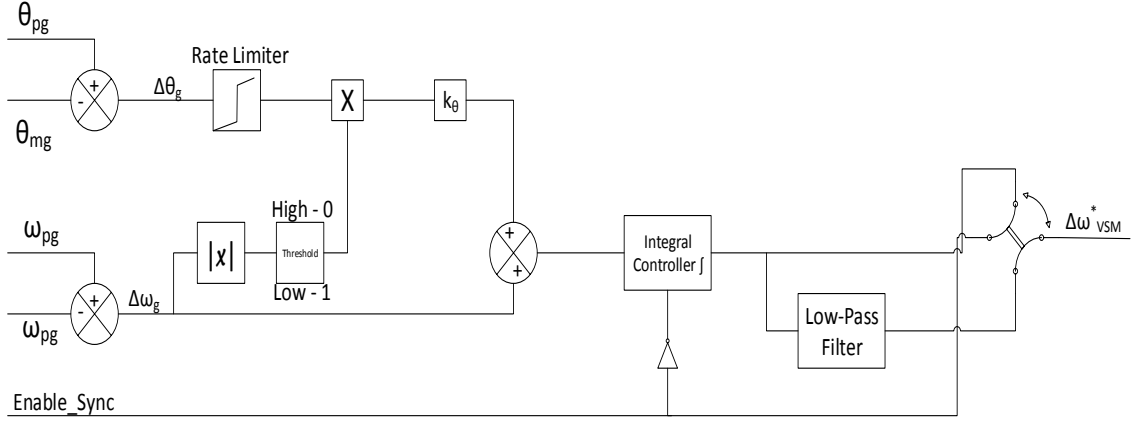


Figure 3.13 Block Diagram of Synchronization Controller

The synchronization controller controls the phase and frequency difference between the microgrid and main utility grid simultaneously, when the frequency difference is below the threshold value. If the frequency difference is above the threshold value, the control action to synchronize the phase will introduce discontinuities and create disturbances. Hence the controller will first try to synchronize the frequency and bring the frequency difference below the threshold value. The integral controller output at this point will be given by equation,

$$\Delta\omega^*_{VSM} = \frac{k_i}{s} \Delta\omega_g. \quad (3.15)$$

When then the frequency difference is sufficiently low, the phase difference would drift between  $-\pi$  and  $\pi$  with a rate given by frequency deviation between the voltages. To avoid the potential oscillations in the activation of the phase angle controller, a small hysteresis is included in the activation of the phase angle input to the controller. The integral

controller output, when it takes the phase and frequency difference input simultaneously is given by

$$\Delta\omega^*_{VSM} = \frac{k_i}{s} (\Delta\omega_g + k_\theta \Delta\theta_g). \quad (3.16)$$

When the phase difference between the microgrid and the main utility grid at PCC is between 0 and 0.1 rad, the signal is sent to the microgrid central controller for the breaker operation for reconnection of microgrid to the main grid. Microgrid central controller monitors the phase difference for about 6 seconds and if the value is within the limit for that time period, then it sends the signal to close the breaker at PCC and connect the microgrid to the main utility grid. Once the microgrid is connected to the grid, the incremental frequency reference  $\Delta\omega^*_{VSM}$  is set to zero. The simulink block diagram in figure 3.14 shows virtual synchronous machine based fuzzy V-F control with cascade synchronization controller.

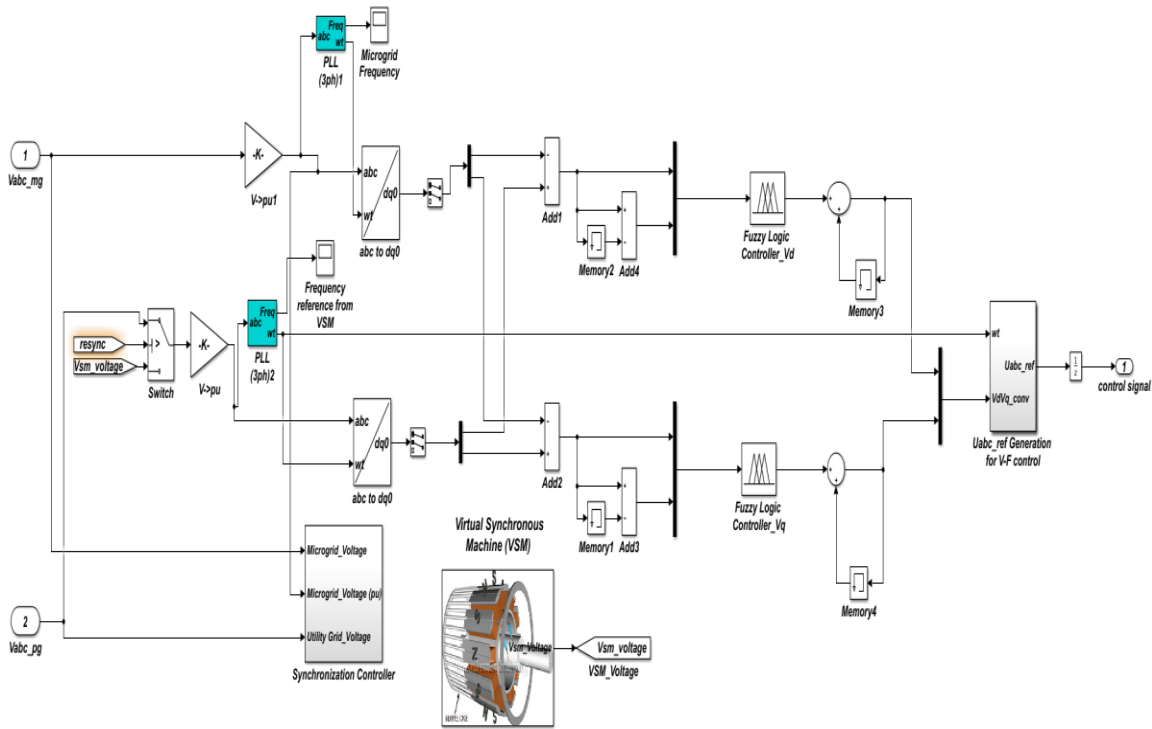


Figure 3.14 Simulink Model of VSM based Fuzzy V-F Control

The table 3.5 displays microgrid test model parameters considered for simulation.

Table 3.5 Microgrid Test Model Parameters

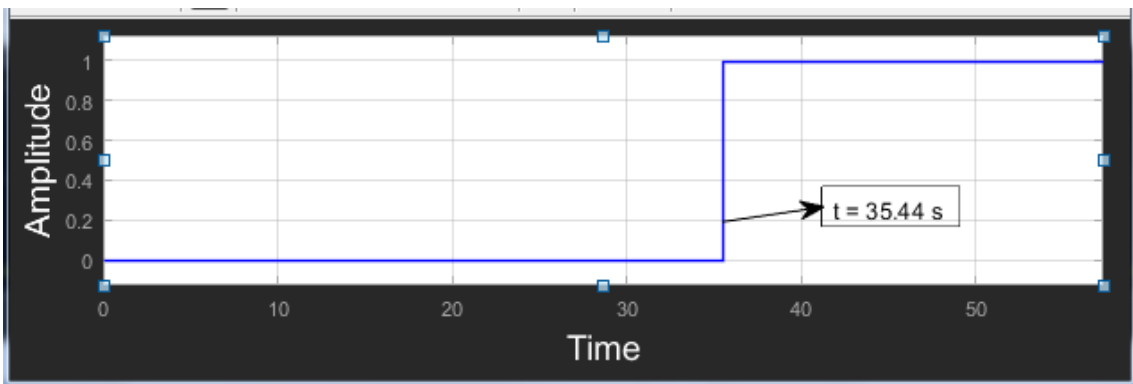
Parameter	Value	Parameter	Value
Inductance (LC Filter)	250 $\mu$ H	Rated Power (VSM)	100 kVA
Capacitance (LC Filter)	10 kVAR	Inertia (VSM)	0.6 s
Kp (Voltage regulator – P-Q control for PV unit)	2	Virtual Load (VSM)	50 KW, 20 kVAR
Ki (Voltage regulator – P-Q control for PV unit)	400	Saturation limit for phase difference (VSM)	$\pm 0.1 \pi$
Kp (Current control inner loop – P-Q control for PV unit)	0.3	Upper threshold for frequency difference (VSM)	7.536 rad
Ki(synchronization controller)	0.004	Phase gain ( $k\theta$ – VSM)	$8 \times 10^{-4}$
Ki (Current control inner loop – P-Q control for PV unit)	20	Lower threshold for frequency difference (VSM)	3.768
Rated Voltage (VSM)	4.16 kV	Maximum allowable frequency rate of change (VSM)	1.502 rad/s
Battery SOC allowable limit	20 %	PLL time constant (VSM)	11 ms

### 3.3.2 Simulation Results

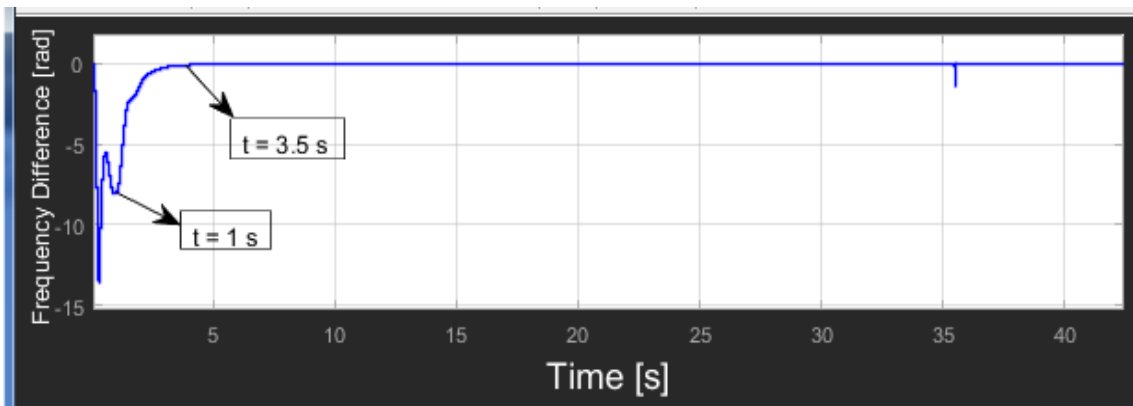
#### 3.3.2.1 Case 1: Seamless Transition of Microgrid from Islanded mode to Grid Connected Mode

The performance of VSM based fuzzy V-F control and synchronization controller is validated in this case for seamless transition of microgrid from islanded mode to grid

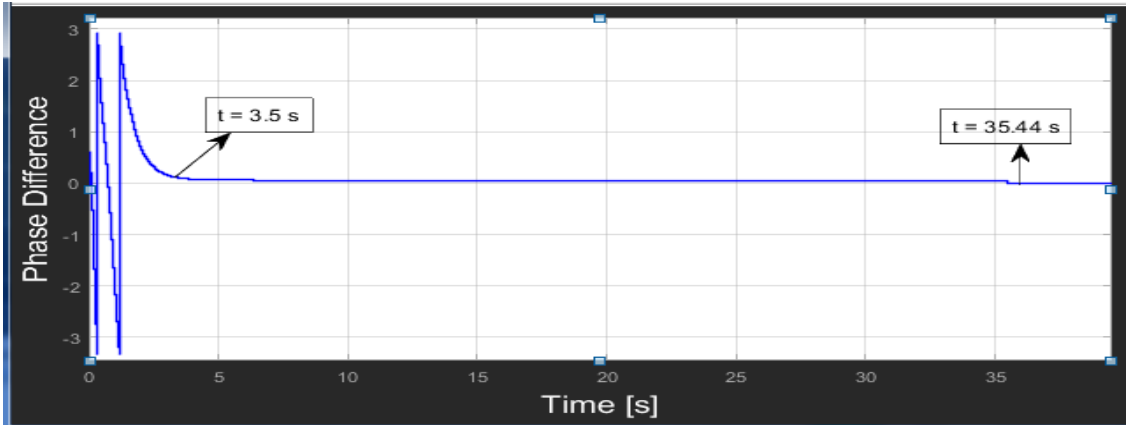
connected mode. The microgrid is operating in islanded mode for few hours and after that microgrid central controller receives a signal for reconnection with the main utility grid. The synchronization control is enabled at  $t = 1$  s to synchronize the microgrid with the main utility grid before reconnection. As explained in previous chapter the synchronization controller will first regulate the frequency difference below the threshold value before it controls the phase difference. During the islanded mode operation of microgrid, it receives the frequency reference from the VSM, which is 61.2 Hz, which is higher than the utility grid frequency of 60 Hz. Hence due to this, the phase difference between the microgrid and the main utility grid at PCC oscillates between  $\mp\pi$  rad. The results of the simulation are shown in figure 3.15. The results of fuzzy controller is compared with the results of PI controller in figure 3.16.



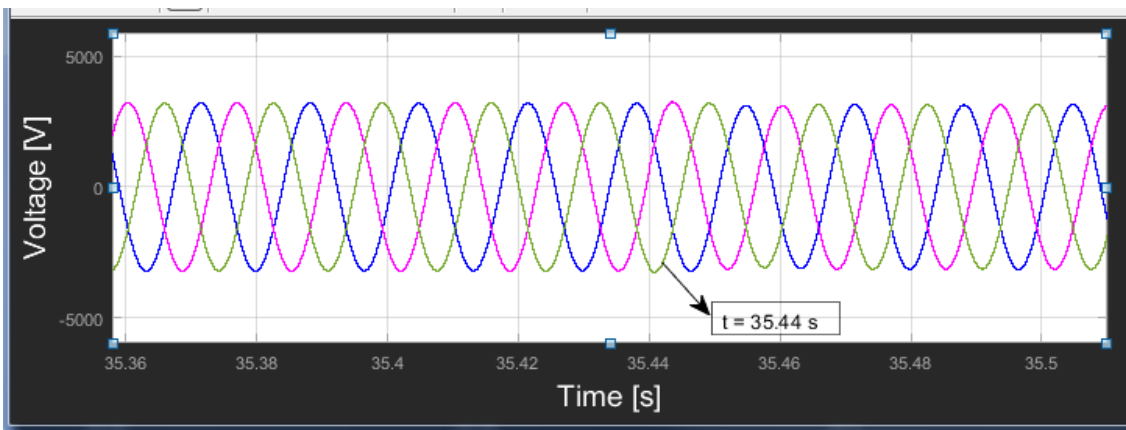
(a)



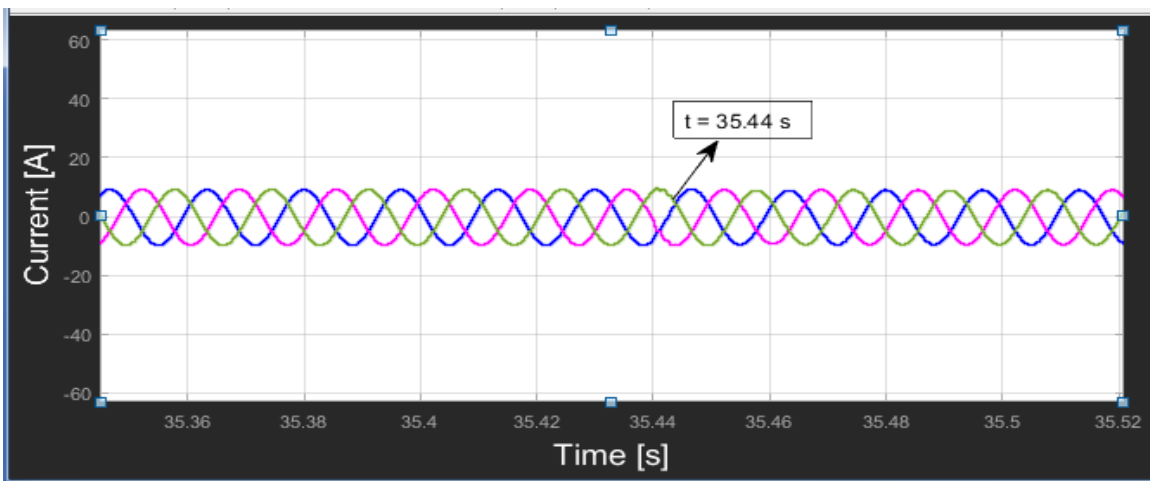
(b)



(c)

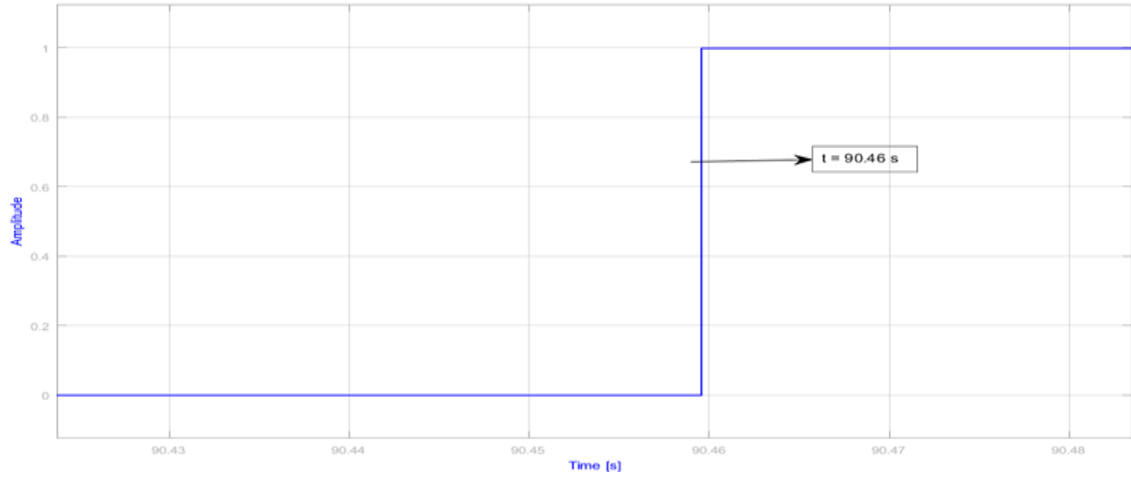


(d)

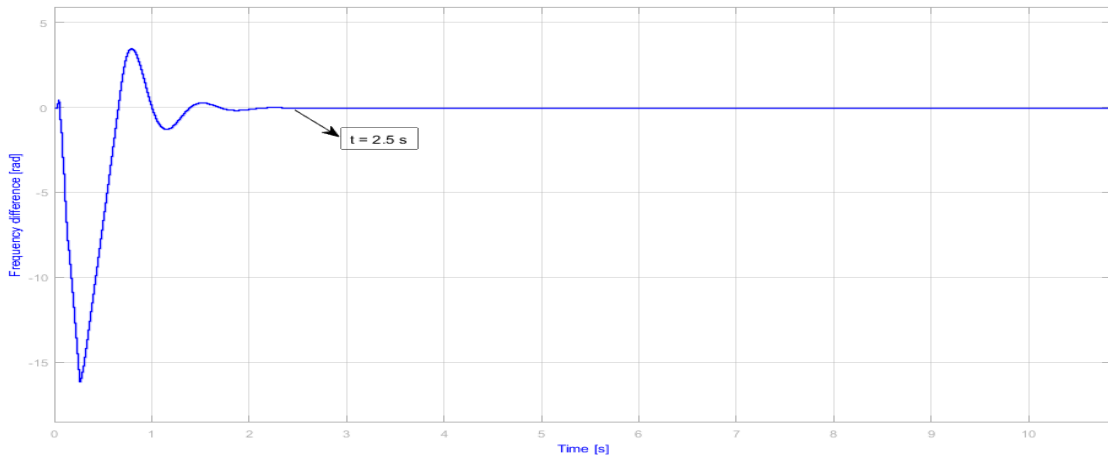


(e)

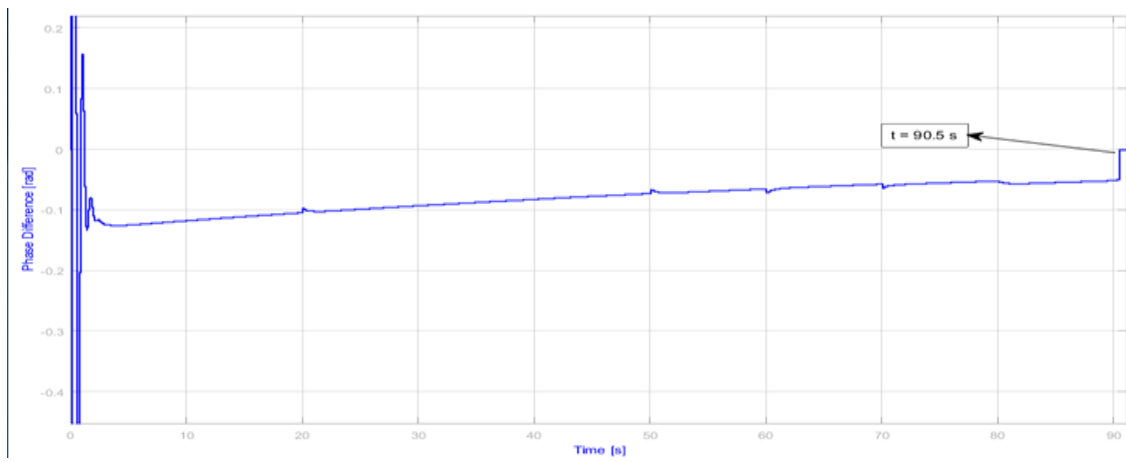
Figure 3.15 (a) Enable signal for reconnection at  $t = 35.44$  s, (b) Frequency synchronization from  $t = 1$  s to  $t = 3.5$  s, (c) Phase Difference Control for  $t = 3.5$  s to  $t = 35.44$  s, (d) Voltage at PCC during Reconnection to Grid at  $t = 35.44$  s and (e) Current at PCC during Reconnection to Grid at  $t = 35.44$  s



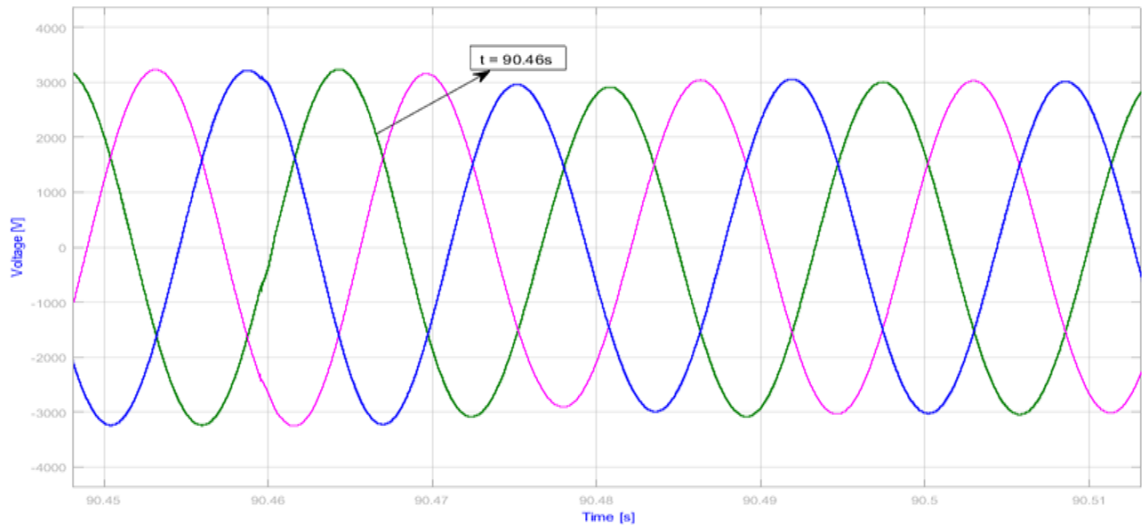
(a)



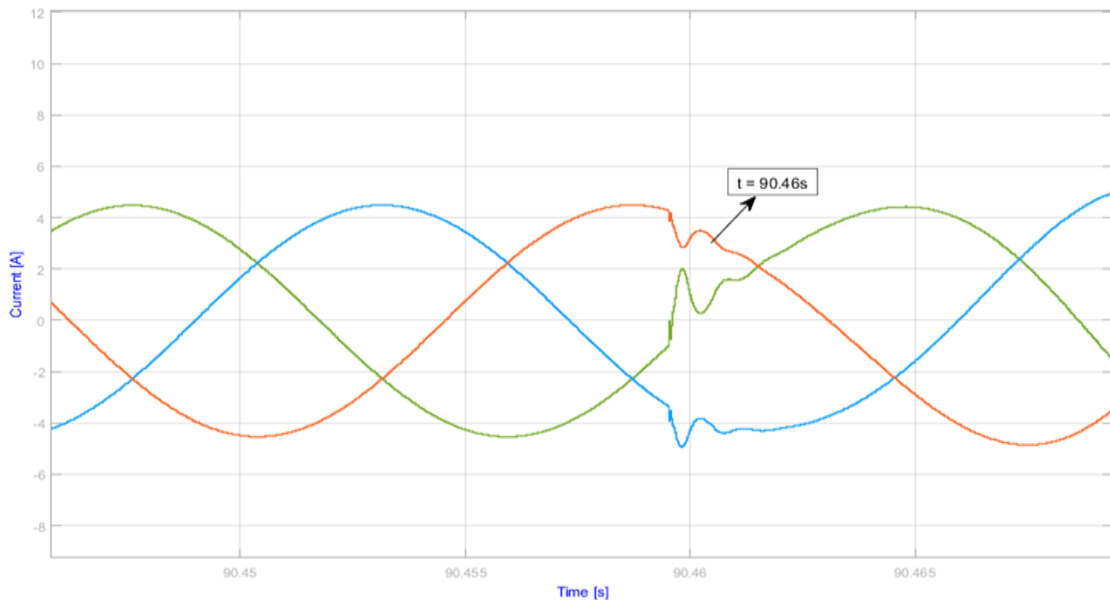
(b)



(c)



(d)



(e)

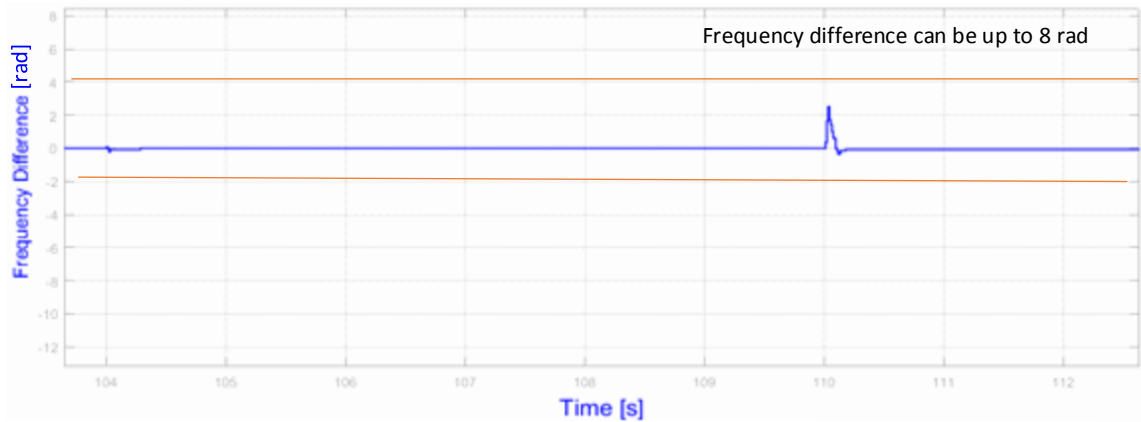
Figure 3.16 (a) Enable signal for reconnection at  $t = 90.46$  s, (b) Frequency synchronization from  $t = 1$  s to  $t = 2.5$  s, (c) Phase Difference Control for  $t = 2.5$  s to  $t = 90.46.44$  s, (d) Voltage at PCC during Reconnection to Grid at  $t = 90.46$  s and (e) Current at PCC during Reconnection to Grid at  $t = 90.46$  s

In this case the reconnection signal is given to the microgrid central controller at  $t=1$  s and it enables the synchronization controller. As soon as the synchronization controller is enabled it acts on the frequency difference first. It is clear from the results that in about 2.5 seconds the frequency difference is compensated and then the controller acts on the phase angle difference to make it zero. It takes about 30 seconds for the phase difference to become zero. As per the IEEE standard 1547.4-2011, the island interconnection device may delay reconnection for up to five minutes, to make sure that voltage, frequency and phase angle of the microgrid and the main utility grid is within the acceptable limits. Thus the proposed controller reconnects the microgrid seamlessly to the main grid at  $t=35.44$  s following the IEEE standard.

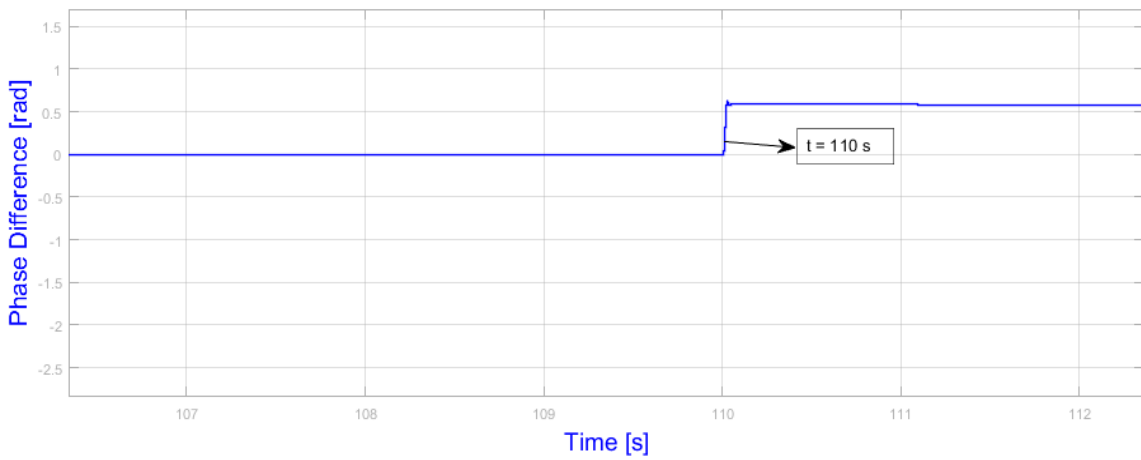
### **3.3.2.2 Case 2: Seamless Transition of Microgrid from Grid-Connected mode to Islanded mode**

Previous case explained the transition of microgrid from islanded mode to grid connected mode. The results shows the seamless integration of microgrid with the main grid after resynchronization at  $t = 35.44$  s. Now the microgrid operates in grid-connected mode and it receives all the reference values from the grid. At  $t = 110$  s fault occurs in the main grid and the microgrid is disconnected from the main grid at PCC. When the fault is detected, the signal is sent to the microgrid central controller for islanding. Then microgrid central controller sends a signal to the breaker at PCC and the breaker open to disconnect microgrid from main utility grid. However, at the instant of islanding, the microgrid voltage and frequency reference is switched to VSM from grid PLL. The new reference values obtained ensures stability of voltage, frequency and active power flow in the microgrid. The results

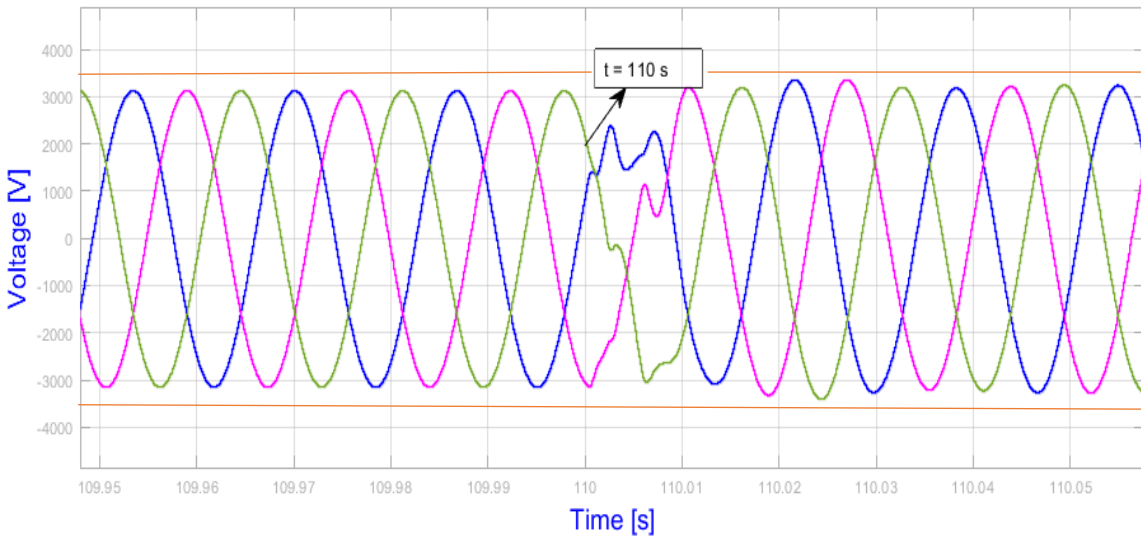
shown in figure 3.16 represents the response of the controller during the transition of microgrid from grid connected mode to islanded mode.



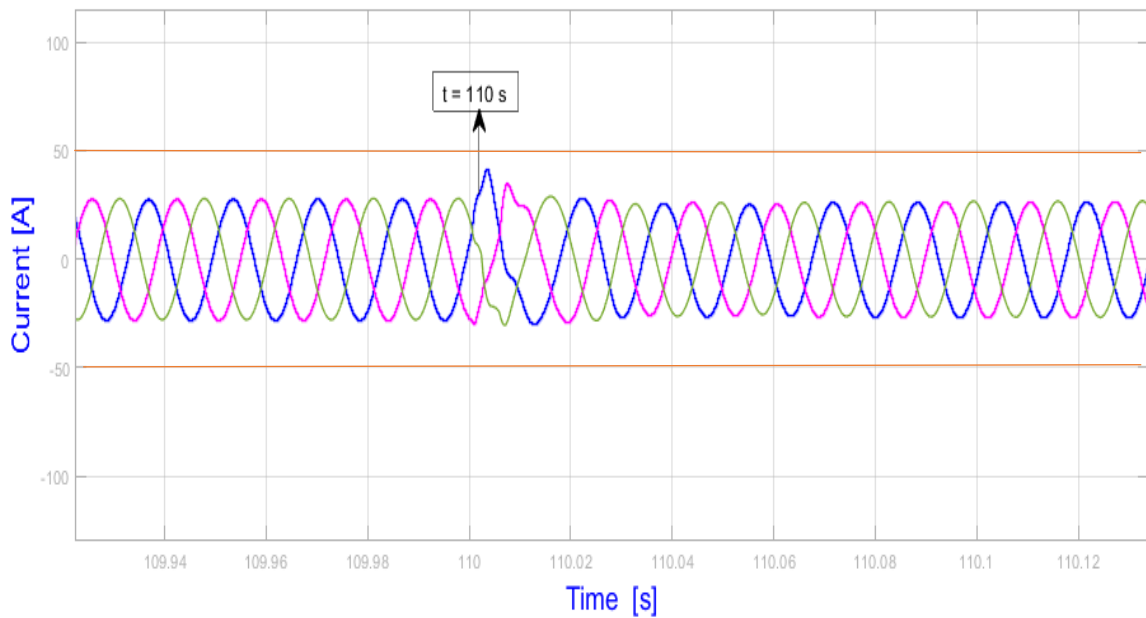
(a)



(b)



(c)



(d)

Figure 3.16 (a) Frequency during Transition from Grid Connected to Islanded Mode at  $t = 110$ s, (b) Phase Difference during Transition from Grid Connected to Islanded Mode at  $t = 110$ s, (c) Voltage during Transition from Grid Connected to Islanded Mode at  $t = 110$ s, and (d) Current during Transition from Grid Connected to Islanded Mode at  $t = 110$ s

It is clear from the results that the islanding of microgrid is successful and within the IEEE standards (IEEE 1547-2003 4.4, Section 8.4.1.2.1, 8.4.1.3.3 and 8.4.1.3.5) [26]. The simulation of the test model is performed with discrete Tustin/Backward Euler solver type in Simpower system with a sample time of  $10 \mu\text{s}$ .

### 3.4 Microgrid Central Controller

The major role of central control system of microgrid is to coordinate generation of DERs and energy storage system and perform load management by feeding the critical load and shedding non critical load during off peak generation in islanded mode. Another role of central control system is to detect islanding during fault condition in the main utility grid and disconnect the microgrid from the main utility by sending a control signal to open the breaker at PCC. During the islanded mode, when microgrid central control system receives a signal for reconnection from the main utility grid, it enables the resynchronization control and it monitors the system until it is perfectly synchronized with the main utility grid before it sends out a control signal to reclose the breaker at PCC. The figure 3.17 shows the simulink block diagram of control system for islanding detection and resynchronization monitoring before reconnection.

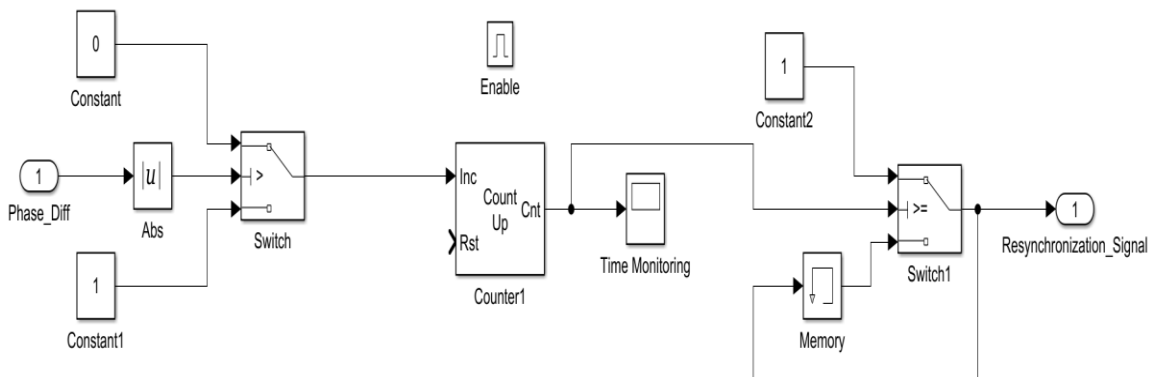


Figure 3.17 Simulink Model of Microgrid Central Controller

The simulation results of load flow in case 3, 4 and 5 will validate the performance of microgrid central controller for load management in islanded mode of operation of microgrid.

### 3.4.1 Simulation Results

#### 3.4.1.1 Case 3: Microgrid Load Management when Demand $[P_{load}] \leq$ Generation $[P_{GenTotal} (P_{PV} + P_{Bat})]$

The microgrid operates in islanded mode up to  $t = 35.44$  s in this simulation. The microgrid local load is defined in load table shown in chapter 2. Along with the local load, there is one critical load of 20kW present in the microgrid which needs to be fed 24 hours a day. The 9<sup>th</sup> hour of the day is considered for simulation to validate the microgrid central controller load management coordination during islanded operation. The figure 3.18 shows the solar irradiance and temperature during the 9<sup>th</sup> hour of the normal sunny day.

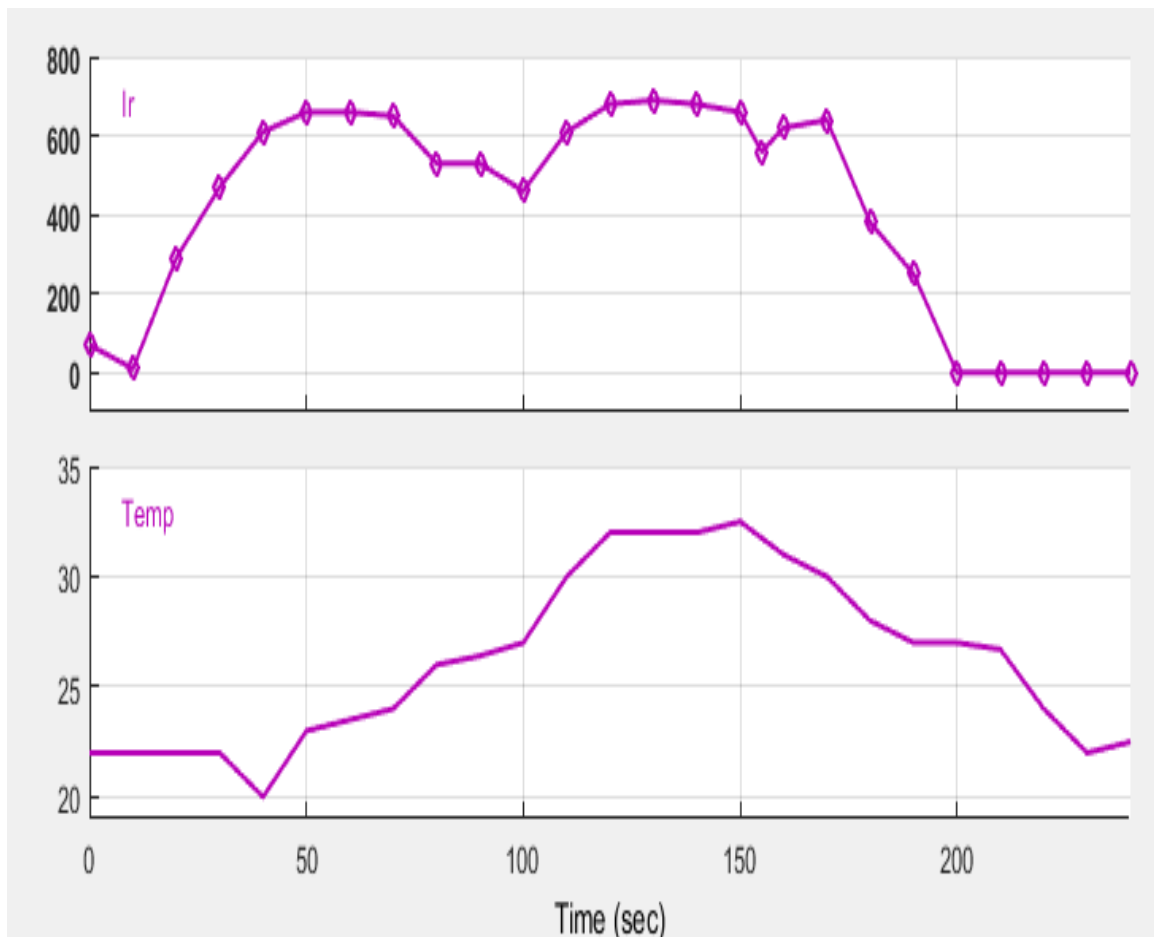
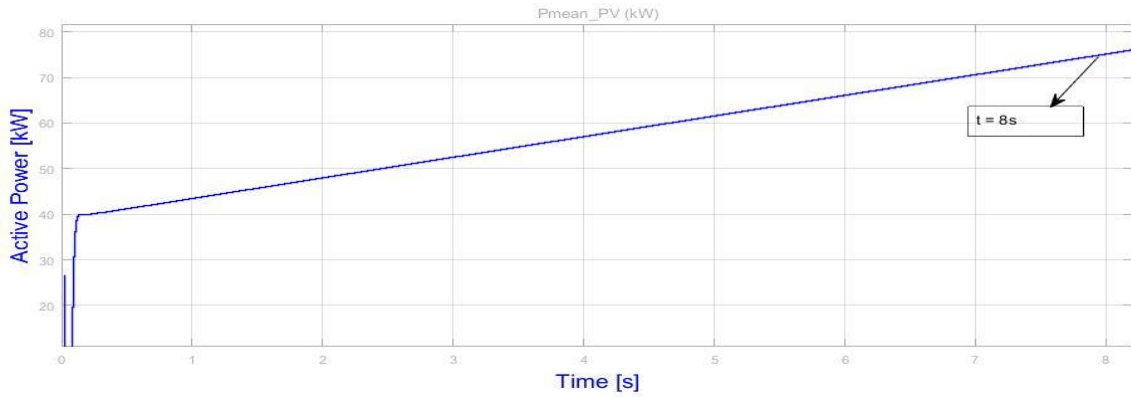
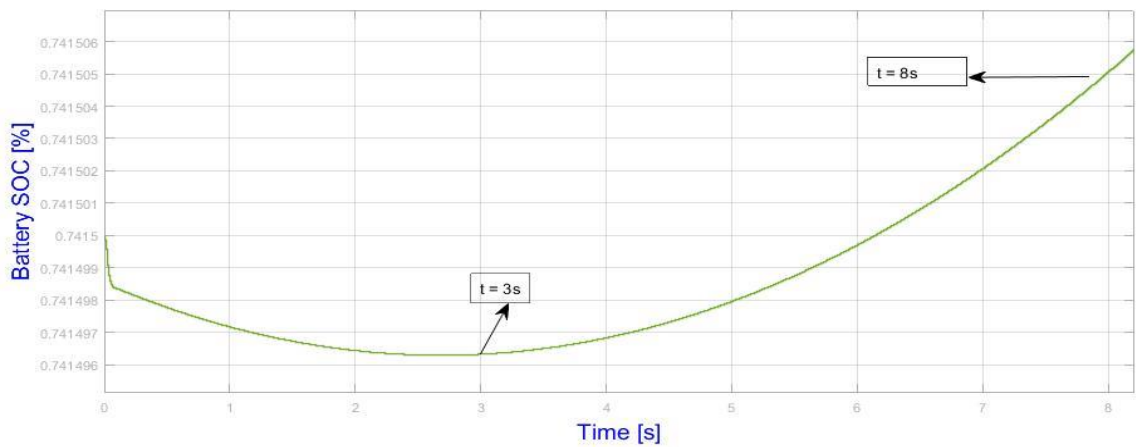


Figure 3.18 Irradiance and Temperature for 24 Hours starting with 9<sup>th</sup> Hour of Day

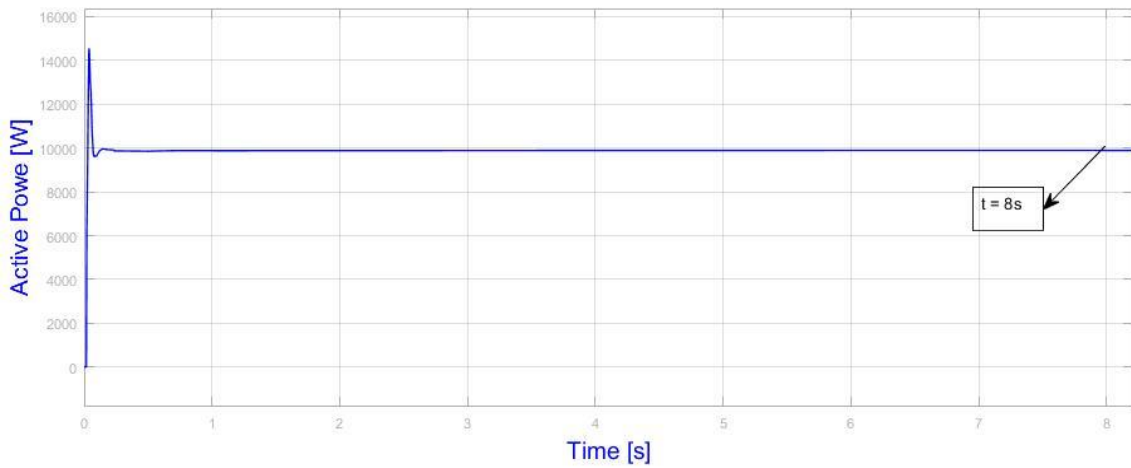
During this hour of the day, battery state of charge percentage is 75% and generation from PV array is about 60 to 70 kW. The figure 3.19 shows the power flow results in islanded microgrid from  $t=1$  s to  $t=8$  s. (Scale: 1 hour of day = 10s simulation time)



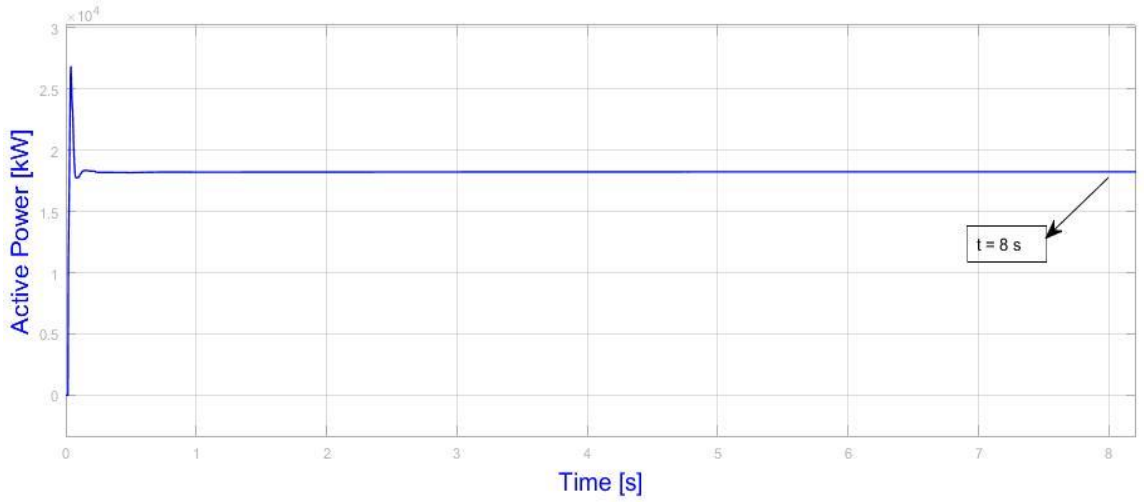
(a)



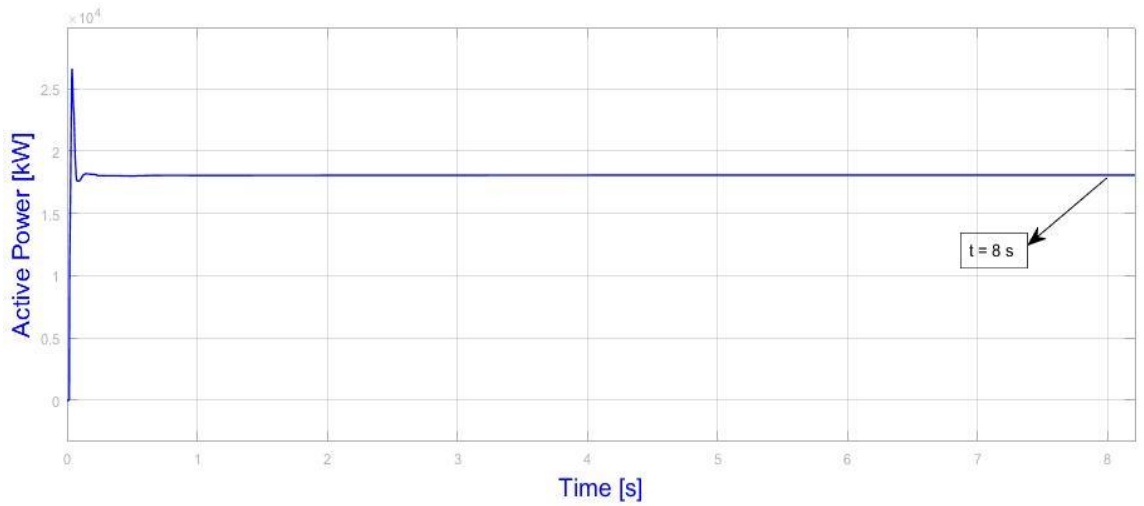
(b)



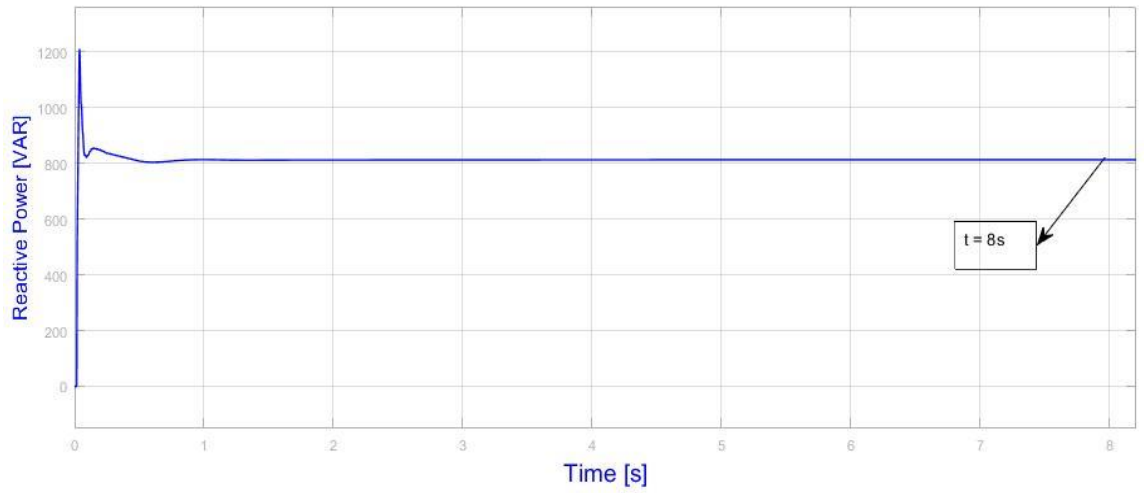
(c)



(d)



(e)



(f)

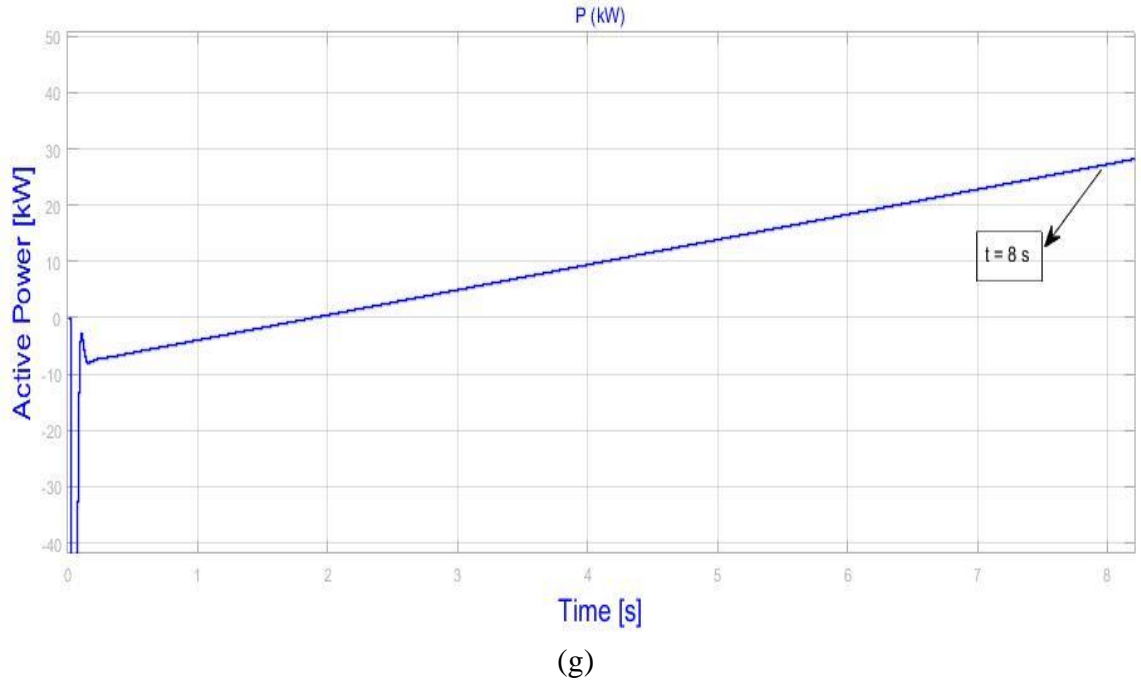


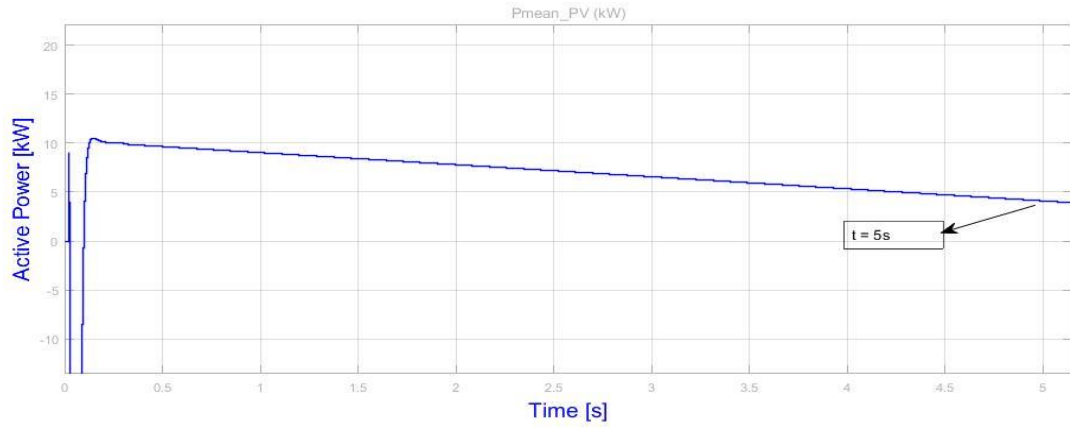
Figure 3.19 (a) Active Power Generation by PV at 9<sup>th</sup> Hour of Day, (b) Battery SOC % at 9<sup>th</sup> Hour of Day, (c) Active Power Feed to Domestic Load at 9<sup>th</sup> Hour of Day, (d) Active Power Feed to Commercial Load at 9<sup>th</sup> Hour of Day, (e) Active Power Feed to Critical Load at 9<sup>th</sup> Hour of Day, (f) Reactive Power of Critical Load at 9<sup>th</sup> Hour of Day and (g) Active Power Flow in Microgrid at PCC

It is clear from the results that up to  $t = 3$  s, PV generation unit is not able to meet the load demand and hence battery energy storage system discharges and feed the load. After  $t = 3$  s there is surplus power from the PV generation unit and it is stored in the battery.

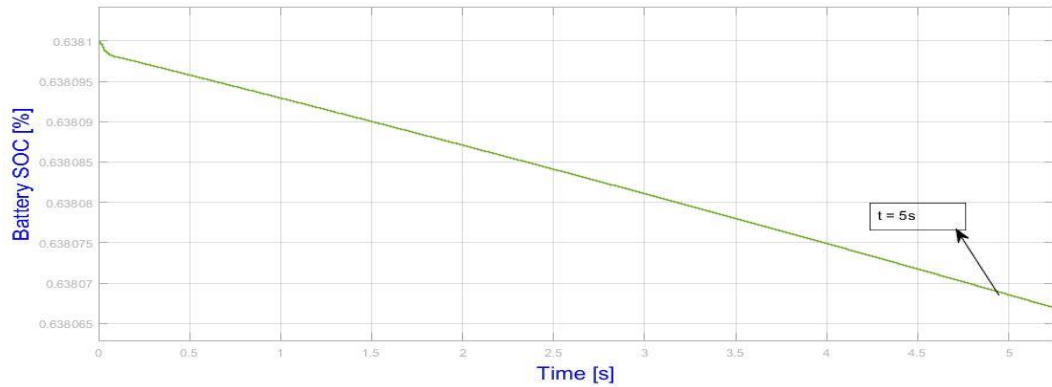
### 3.4.1.2 Case 4: Microgrid Load Management when Photovoltaic Generation $[P_{PV}] \sim 0$ kW & Battery Energy Storage System Power $[P_{Bat}] > Demand [P_{Load}]$

Unlike the previous case, during 9<sup>th</sup> hour of the day if it partial or fully cloudy then PV generation unit will not be able generate any power or will generate negligible power, maybe up to 10kW in this case. If battery energy storage system is charged up to 65% from

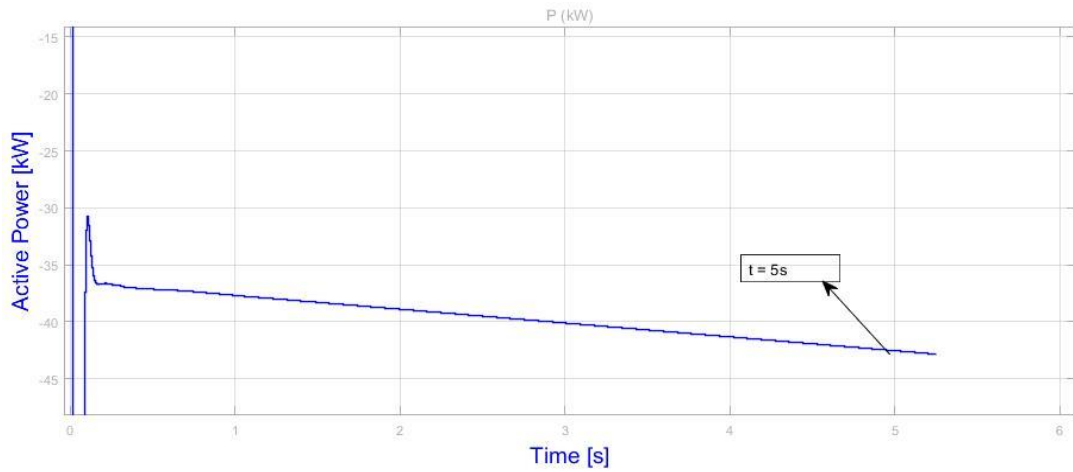
the previous day, then it will feed all the local loads. The figure 3.20 shows the power flow in the system from  $t = 0$ s to  $t = 5$ s. (Scale: 1 hour of day = 10s simulation time)



(a)



(b)



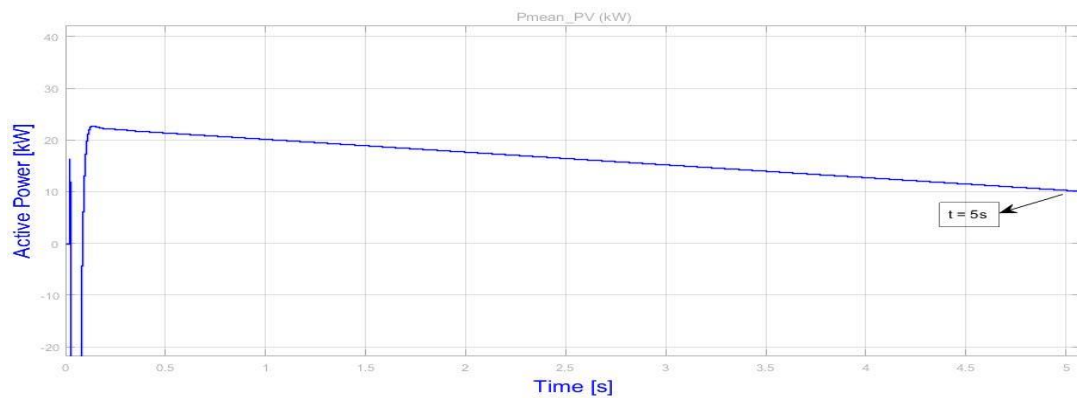
(c)

Figure 3.20 (a) Active Power Generation by PV at 9<sup>th</sup> Hour of Cloudy Day, (b) Battery SOC % at 9<sup>th</sup> Hour of Cloudy Day, and (c) Active Power Flow in Microgrid at PCC

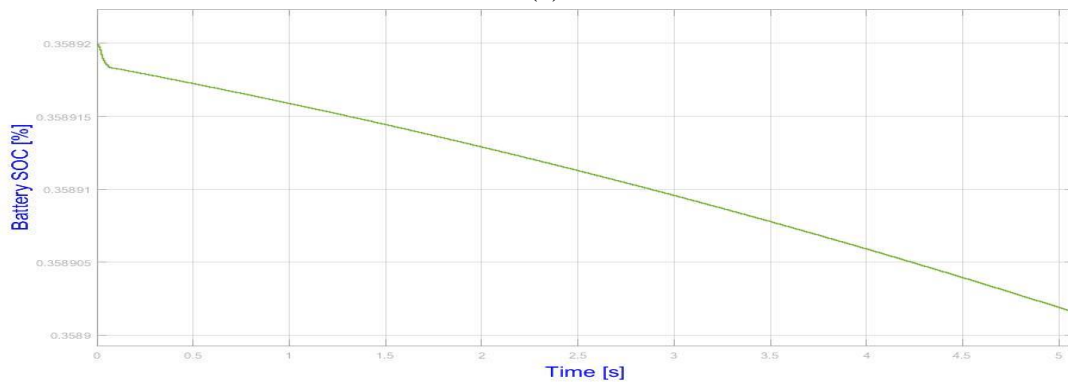
### 3.4.1.3 Case 5: Microgrid Load Management when Photovoltaic

#### Generation [ $P_{PV}$ ] $\sim 0$ kW && Battery<sub>SOC</sub> < 40%

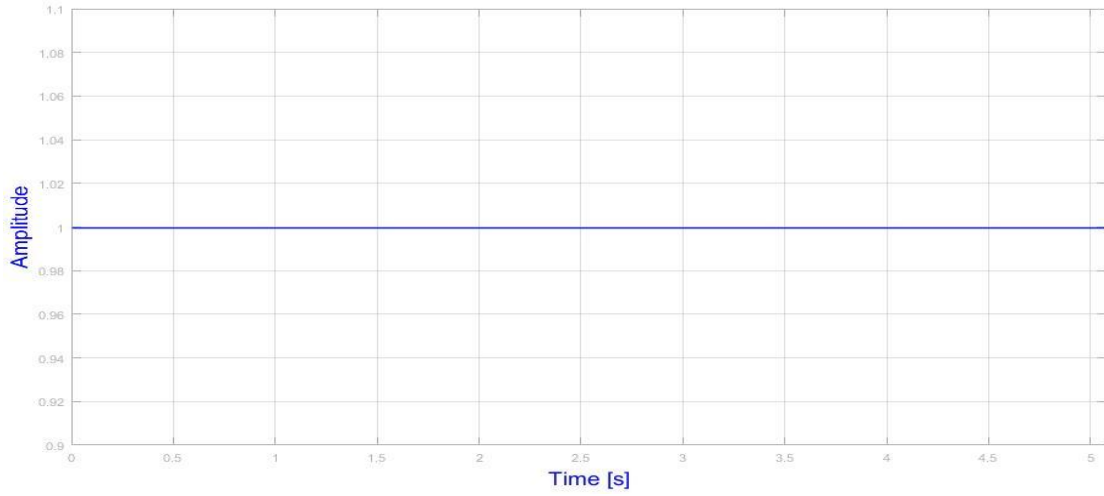
In this case, let us say that there is no generation by PV array and also battery energy storage system is not charged i.e. battery SOC is less than 40 %, then microgrid central controller will send a signal to shed the load based on priority. Here, in this case, if battery SOC is less than 40% but greater than 35% it will shed domestic load and if battery SOC is less than 35 % but greater than 30 % it will shed domestic as well non critical commercial load. But if battery SOC is less than 30%, it will shed all the local loads and battery will only feed the critical load in the system. For simulation, battery SOC is 38 % and results in figure 3.21 shows that microgrid central controller sends a signal to shed domestic load.



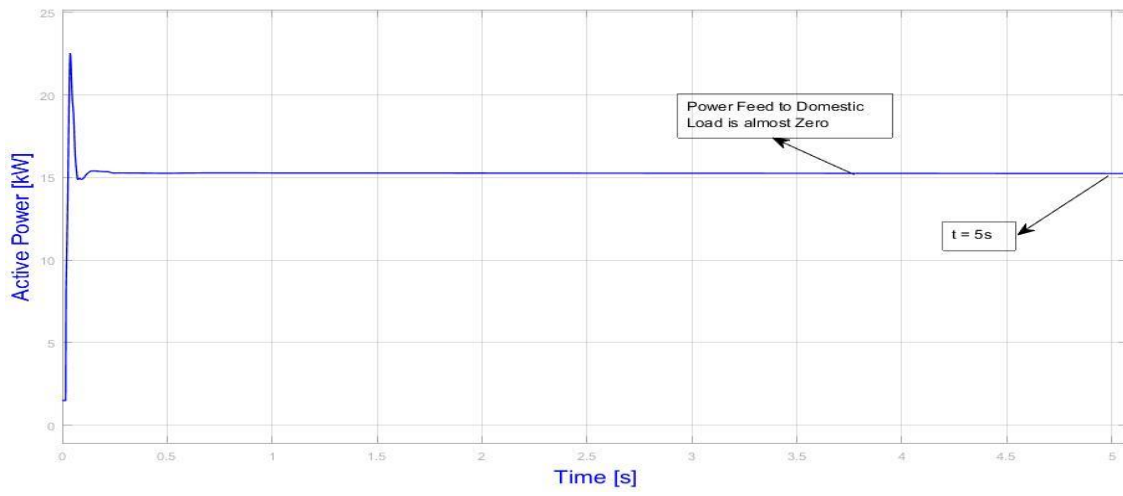
(a)



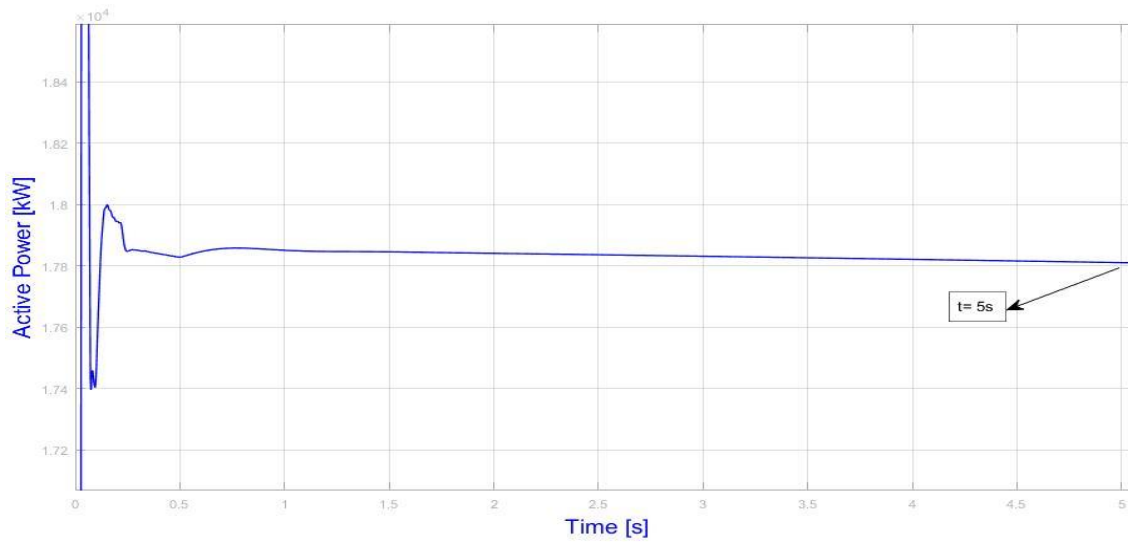
(b)



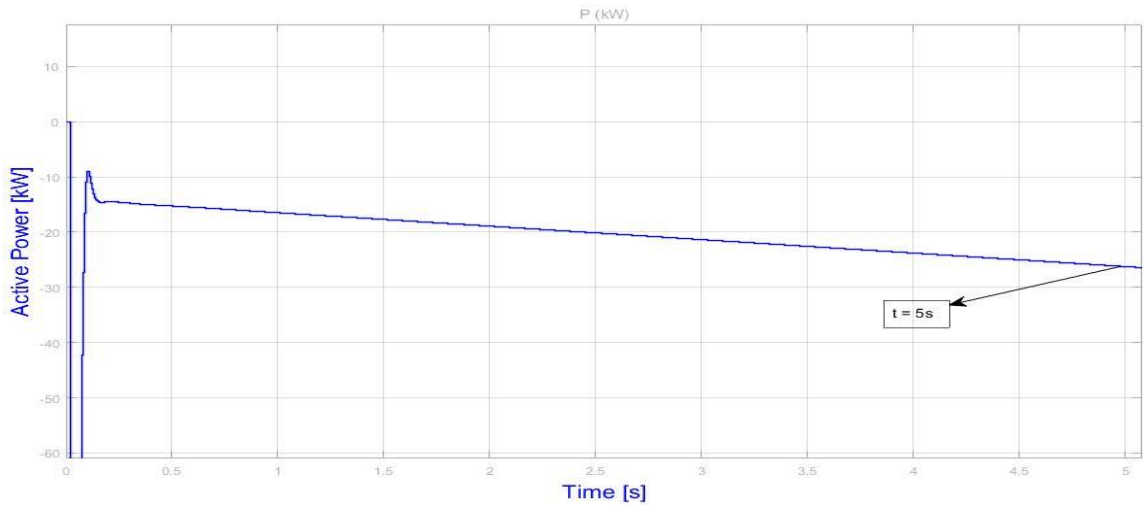
(c)



(d)



(e)



(f)

Figure 3.21 (a) Active Power Generation by PV at 9<sup>th</sup> Hour of Day, (b) Battery SOC % at 9<sup>th</sup> Hour of Day, (c) Microgrid Central Controller Signal to Shed Domestic Load, (d) Active Power Feed to Domestic Load at 9<sup>th</sup> Hour of Day, (e) Active Power Feed to Commercial Load at 9<sup>th</sup> Hour of Day, (f) Active Power Flow in Microgrid at PCC

## CHAPTER 4 CONCLUSION

The proposed VSM based fuzzy control method for the control of power electronic converters of battery energy storage system in both islanded and grid connected mode of operation of microgrid is successfully validated by simulation results of all the five cases. This thesis work presents P-Q control for PV generation system in grid connected mode which obtains the voltage and frequency reference from the grid and successfully tracks the maximum power from the PV generation unit. Thus it ensures seamless performance of microgrid in grid connected mode and the results from case 2 validates it. The proposed VSM based Fuzzy V-F control for energy storage system power converter and cascade synchronization controller ensures the seamless performance of microgrid in islanded mode, seamless transition from islanded mode to grid connected mode and vice versa. The purpose of VSM implementation is to emulate power electronic converters like conventional synchronous machines to maintain the frequency and phase angle reference in converter based microgrid as demonstrated in this work. Also, microgrid central controller detects islanding, manages energy storage power dispatch and performs load management. The energy storage system power dispatch and load shedding under various scenarios is presented by the results in case 3, 4 and 5. Finally, the system is tested only for few cases under limited number of scenarios, the proposed control topology is suitable for various other conditions too. The system is tested and verified by performing simulation in MATLAB/Simulink environment.

## REFERENCES

- [1] D. T. Ton and M. A. Smith, “The U.S. department of energy’s microgrid initiative,” *The Electricity Journal*, Elsevier, 2012.
- [2] L. Chang, C. Diduch and P. Song, “Development of standards for interconnecting distributed generators with electric power systems,” *IEEE Power Electronics Specialists Conf.*, June 2005, pp. 2501-2507
- [3] S. Hung Hu, C. Yi Kuo, T. Lin Lee and J. M. Guerrero, “Droop-controlled inverters with seamless transition between islanding and grid-connected operations,” Joseph M. Guerrero Dept. Energy Technology Aalborg University DENMARK, 2011 *IEEE*
- [4] A. T. Moore and J. Jiang, “Design and implementation of a microgrid controller for bumpless transitions between grid-connected and island operation,” *IECON 2014 – 40<sup>th</sup> annual conference of IEEE*, Dallas, TX, U.S.A.
- [5] B. Bahrani, M. Saeedifard, A. Karimi, and A. Rufer, “A multivariable design methodology for voltage control of a single- DG-unit microgrid,” *IEEE Trans. Ind. Informat.*, vol. 9, no. 2, pp. 589–599, May 2013.
- [6] Y. Li and M. Wang, “Control Strategies for grid-connected and island dual mode operated Inverter under Unbalanced Grid Voltage Conditions,” *2012 IEEE 7th International Power Electronics and Motion Control Conference – ECCE*.
- [7] L. Priyadarshane, “Modelling and control of hybrid AC/DC microgrid,” Master’s thesis, Department of Electrical Engineering, National Institute of Technology, Rourkela.

- [8] H. Fathima and K. Palanisamy, "Optimized sizing, selection, and economic analysis of battery energy storage for grid-connected wind-PV hybrid system," Hindawi publishing corporation, modelling and simulation in engineering, Vol. 2015, Article ID 713530.
- [9] <http://www.tesvolt.com/assets/files/documents/TESVOLT-Eng-TLC-datasheet.pdf>
- [10] S. Bacha, I. Munteanu, and A. L. Bratcu, "Power electronic converters modelling and control," Springer – Verlag London, 2014.
- [11] K. Bendaoud, J. Laassiri, S. Krit, and L. Maimouni, "Design and simulation DC-DC power converters buck and boost for mobile applications using Matlab/Simulink," IEEE International conference on engineering and MIS ICEMIS 2016.
- [12] H. S. Ramirez, and R. S. Ortigoza, "Control design techniques in power electronics devices," Springer, pp 11-58, 2006.
- [13] "Basic calculation of a boost converter's power stage," Texas Instruments, Application report SLVA372C, January 2014.
- [14] J. P. Rodriguez, "Dynamic averaged models of VSC-based HVDC systems for electromagnetic transients programs," PhD dissertation, University de Montreal, August 2013.
- [15] C.K.A.E. Fitzgerald, S. D. Umans, "Electrical Machinery," 6<sup>th</sup> Edition, McGraw-Hill, 2003.
- [16] A. Perera, "Virtual synchronous machine based power control in active rectifiers in

- microgrid (MSc. Thesis),” Norwegian university of Science and Technology, July 2012.
- [17] J. Machowski, J. Bialek and J. Bumby, “Power system dynamic: stability and control,” Second Edition, John Wiley & Sons, November 2008.
- [18] M. Jamshidi, N. Vadiiee and T. J. Ross, “Fuzzy logic and control: software and hardware applications,” Prentice hall, 1<sup>st</sup> Edition, June 1993.
- [19] J. Yen, R. Langari, “Fuzzy logic: intelligence, control, and information,” Pearson, 1<sup>st</sup> Edition, November 1998.
- [20] L. Wang, “A course in fuzzy systems and control,” Prentice Hall, 1<sup>st</sup> Edition, August 1996.
- [21] H. A. Malki and C. Umeh, “Design of fuzzy-logic based level controller,” Journal of Engineering Technology, Vol. 17, no. 1, pp. 32-38, Spring 2000.
- [22] H. P. Beck and R. Hesse, “Virtual synchronous machine,” 9<sup>th</sup> International conference, Electrical power quality and utilization, Barcelona, October 2007.
- [23] S. D’Arco, J. A. Suul and O. B. Fosso, “A virtual synchronous machine implementation for distributed control of power converters in smart grid,” Electric power systems research (ELSEVIER), February 2015.
- [24] S. D’Arco and J. A. Suul, “A synchronization controller for grid reconnection of islanded virtual synchronous machine,” IEEE 6<sup>th</sup> International symposium on power electronics for distributed generation system (PEDG), August 2015.
- [25] B. M. Hamed, M. Moghany, “Fuzzy Control Design Using FPGA for Photovoltaic

Maximum Power Point tracking,” International journal of advanced research in artificial intelligence, Vol. 1, No.3, 2012.

[26] “IEEE application guide for IEEE std. 1547, IEEE standard for interconnecting distributed resources with electric power systems,” IEEE Std. 1547.2, 2008.

[27] L.A. Zadeh, “Fuzzy sets,” Elsevier Information and Control, Vol. 8, Issue 3, pp. 338-353, June 1965.

[28] E. H. Mamdani and S. Assilian, “An experiment in linguistic synthesis with a fuzzy logic controller,” International journal of man-machine studies, vol.7, No. 1, pp. 1-13, 1975.

